Transport and Storage of Potassium in the Earth□s Upper Mantle and Transition Zone: an Experimental Study to 23 GPa in Simplified and Natural Bulk Compositions

Article *in* Journal of Petrology · April 2000

DOI: 10.1093/petrology/41.4.583 · Source: OAI

CITATIONS
60

READS
70

2 authors:

Jürgen Konzett
University of Innsbruck
108 PUBLICATIONS **1,768** CITATIONS
SEE PROFILE

Yingwei Fei
Carnegie Institution for Science
506 PUBLICATIONS **13,288** CITATIONS
SEE PROFILE

JOURNAL OF PETROLOGY | VOLUME 41 | NUMBER 4 | PAGES 583–603 | 2000

Transport and Storage of Potassium in the Earth's Upper Mantle and Transition Zone: an Experimental Study to 23 GPa in Simplified and Natural Bulk Compositions

JÜRGEN KONZETT* AND YINGWEI FEI

GEOPHYSICAL LABORATORY AND CENTER FOR HIGH-PRESSURE RESEARCH, CARNEGIE INSTITUTION OF WASHINGTON, 5251 BROAD BRANCH ROAD NW, WASHINGTON DC, 20015-1305, USA

RECEIVED MARCH 22, 1999; REVISED TYPESCRIPT ACCEPTED SEPTEMBER 21, 1999

We have investigated the stability and composition of potassium amphibole and its high-pressure breakdown product phase X in synthetic peralkaline and subalkaline KNCMASH (K_2O–Na_2O–CaO–MgO–Al_2O_3–SiO_2–H_2O) and natural KLB-1 peridotite bulk compositions between 10 and 23 GPa at 800–1800°C. In the KNCMASH system, potassium amphibole reaches its upper pressure stability limit at 13–15 GPa at ≤1400°C. In the natural KLB-1 bulk composition, potassium amphibole breaks down between 12 and 13 GPa at 1200°C. Phase X is a hydrous potassium–magnesium silicate with variable stoichiometry, a general formula $K_{2-x}Mg_2Si_2O_7H_x$ with x = *0–1, and a maximum possible H_2O content of 3·5 wt %. Electron microprobe analytical totals suggest H_2O contents of ~1–2 wt % and a decrease in H_2O contents with increasing pressure. In both KNCMASH and KLB-1 systems, phase X coexists with Mg_2SiO_4 + garnet + high-Ca clinopyroxene + low-Ca clinopyroxene ± fluid. Phase X breaks down between 20 and 23 GPa at 1500–1700°C to form K-hollandite + γ-Mg_2SiO_4 + majorite + Ca-perovskite + fluid. The upper temperature stability limit of phase X was located in the subalkaline KNCMASH system between 1400 and 1600°C at 14 GPa and at >1700°C at 20 GPa, the latter being at least 200°C above an average current mantle adiabat. Thus, phase X could store and transport both water and potassium not only in subduction zone settings, but also in convecting mantle down to the transition zone–lower-mantle boundary. Phase X would also be an eminently suitable host for Rb, Cs, Ba or Pb.*

KEY WORDS: *experimental study; high pressure; phase X; potassium*

INTRODUCTION

The hydrous potassic phases (HPP) phlogopite and K-amphibole are major storage sites for potassium in the Earth's upper mantle. Both host the incompatible trace elements with large ionic radii (Rb, Ba or Pb), which can occupy large and highly coordinated lattice positions in phlogopite and K-amphibole (Basu, 1978; Foley *et al.*, 1995; Ionov *et al.*, 1997). Phlogopite is an important component in sources of kimberlites, lamproites, lamprophyres and K-rich basaltic rocks (e.g. Wilkinson & LeMaitre, 1986; Esperança & Holloway, 1987; Rogers, 1992; Mitchell, 1995, and references therein; Sato, 1997). K-richterite has been suggested as a possible source of K, Ti and high field strength elements (HFSE) for kimberlites and ultrapotassic rocks (Foley, 1992; Taylor *et al.*, 1994). Phlogopite is stable in Al-rich metasedimentary and peridotitic bulk compositions. In Al-rich bulk compositions phlogopite breaks down at relatively low P (and T) to form phengite ± K-feldspar and possibly K,Mg-rich fluid (Massonne & Schreyer, 1989; Massonne, 1992). In peridotitic bulk compositions, phlogopite is stable to at least 6 GPa and 1100°C with orthopyroxene + clinopyroxene + olivine (Konzett & Ulmer, 1999; see also Wendlandt & Eggler, 1980; Mengel & Green, 1989, for experiments at lower P) and to at least 12 GPa and 1350°C with phlogopite + clinopyroxene (Luth, 1997). Phlogopite is stable above the solidus of natural lherzolite at $P \leq 3$ GPa (Wendlandt & Eggler, 1980). Experiments with phlogopite + enstatite (Sato *et al.*, 1997) suggest

*Corresponding author. Present address: Institut für Mineralogie und Petrographie, Universität Innsbruck, Innrain 52, A-6020 Innsbruck, Austria. Telephone: +43-512-507-5506. Fax: +43-512-507-2926. e-mail: juergen.konzett@uibk.ac.at

above-solidus stability of phlogopite through continuous melting reactions between 4 and 8 GPa that form olivine + pyrope. Although it is difficult to distinguish hydrous melts from fluids at high P, K-richterite is likely to be unstable above the solidus in either subalkaline or peralkaline bulk compositions (Konzett *et al.*, 1997; Konzett & Ulmer, 1999). However, K-richterite probably controls the P–T location of the solidus by incongruent melting (Gilbert & Briggs, 1974; Foley, 1991).

K-amphibole with a composition close to KNa$CaMg_5Si_8O_{22}(OH)_2$ can form as a high-P breakdown product of phlogopite in peridotitic bulk compositions at P >6 GPa (Trønnes *et al.*, 1988; Luth, 1997; Konzett & Ulmer, 1999). In Na-free systems the K-amphibole $KKCaMg_5Si_8O_{22}(OH)_2$ is present (Sudo & Tatsumi, 1990; Luth, 1997; Inoue *et al.*, 1998; Yang *et al.*, 1999). In peralkaline bulk compositions [mica–amphibole–rutile–ilmenite–diopside (MARID), lamproites] phase relations from natural rocks and from high-P experiments suggest a continuous stability of K-amphibole + phlogopite from 0·1 MPa to at least 8·5 GPa (Mitchell & Bergman, 1991, and references therein; Konzett *et al.*, 1997).

Experimental studies of the KCMSH and KCMASH systems (Luth, 1997; Inoue *et al.*, 1998) show that K-amphibole breaks down at high pressures to a hydrous K-rich silicate that is capable of transporting alkalis and water to even greater depths than does amphibole. The structure, stoichiometry and compositional variability of this phase—termed phase X (Luth, 1995)—are still unknown and its stability field is poorly constrained. The aims of our study are to (1) better constrain the stability field of phase X, especially its high-pressure stability limit; and (2) determine the chemical variability of phase X and coexisting phases. This will permit us to assess the potential of phase X as a storage site for water and alkalis in the mantle transition zone and to trace mechanisms of potassium and water recycling into the mantle.

COMPOSITION OF STARTING MATERIALS

Our subalkaline and peralkaline starting materials are mixes of high purity (≥99·95% purity) synthetic oxides or silicates and carbonates, and cover the full range of bulk compositions that can stabilize K-amphibole and its breakdown products (Table 1). They represent peridotitic and MARID-type (Dawson & Smith 1977) or lamproitic bulk composition, respectively. The phase relations of these bulk compositions at P <10 GPa have been described by Konzett *et al.* (1997) and Konzett & Ulmer (1999). A simplified K_2O–Na_2O–CaO–MgO–Al_2O_3–SiO_2–H_2O (KNCMASH) system was examined to avoid the potential influence of fO_2 on phase relations in an Fe-bearing system at very high pressures as a result of stabilization of phases by Fe^{3+} partitioning. Despite this simplification, the system is still complex enough to permit all important exchange reactions ($MgSiAl_{-2}$, $NaSiCa_{-1}Al_{-1}$, $CaMg_{-1}$, KNa_{-1}) among the silicate phases. Additional experiments were conducted with KLB-1 peridotite (Takahashi, 1986) doped with 10 wt % synthetic K-richterite, to locate the amphibole → phase X transition in a natural peridotitic bulk composition.

Table 1: Compositions of synthetic and natural starting materials

	KNCMASH subalk bulk	KNCMASH peralk bulk	KLB-1	KLB-1 + 10 wt % Kr
SiO_2	47·28	47·61	44·48	45·67
TiO_2	—	—	0·16	0·15
Al_2O_3	11·50	6·67	3·59	3·27
Cr_2O_3	—	—	0·31	0·28
FeO*	—	—	8·10	7·37
Fe_2O_3	—	—	—	—
MnO	—	—	0·12	0·11
MgO	27·26	23·79	39·22	37·87
CaO	6·58	7·61	3·44	3·74
Na_2O	1·22	1·94	0·30	0·69
K_2O	4·94	7·62	0·02	0·40
P_2O_5	—	—	0·03	0·03
NiO	—	—	0·25	0·23
H_2O	1·22	4·76	—	0·20
Σ	100·00	100·00	100·02	100·01
PI	0·64	1·72		0·48
K/Na	2·66	2·58	0·38	

KLB-1 analysis, Takahashi (1986); composition of synthetic K-richterite (Kr) (average of 10 analyses): SiO_2 57·22(20); MgO 24·20(22); CaO 6·71(19); Na_2O 4·61(09); K_2O 4·16(11); analytical procedure is as given by Konzett & Ulmer (1999); PI (peralkalinity index) = molar $(K_2O + Na_2O)/Al_2O_3$.

EXPERIMENTAL AND ANALYTICAL TECHNIQUES

Experiments (Table 2) were performed with Walker-type and split-sphere MA-8 multianvil devices at the Geophysical Laboratory (GL) and at the Bayerisches Geoinstitut (BG), respectively, using prefabricated pyrophyllite gaskets and MgO octahedra. Assembly sizes and furnace materials are as follows: GL: 10/5 (10 mm edge length of octahedra/5 mm truncated edge length of WC cubes) and 8/3 assemblies to 15 and 23 GPa using Re heaters; BG: 14/7 assemblies using stepped

$LaCrO_3$ heaters. Pre-dried starting materials were placed in 1·55 mm or 1·00 mm (GL, for 8/3 assemblies) outer diameter Pt_{100} capsules and welded shut immediately. For the KLB-1 starting material, an additional inner graphite capsule (approximate dimensions after runs: wall thickness 300 μm, bottom and lid 200 μm) was added. To minimize T gradients and phase separation as a result of thermal diffusion, the length of experimental charges ranged between 200 and 600 μm. T gradients were ~20°C/100 μm for 8/3 assemblies and <10°C/100 μm for 10/5 assemblies (Bertka & Fei, 1997, and unpublished data, 1999). Temperatures were measured with W3%Re–W25%Re thermocouples without correcting for the pressure effect on e.m.f. Both pressure and temperature were computer controlled during the runs. Detailed descriptions of the GL and BG experimental and calibration procedures have been given by Bertka & Fei (1997) and Rubie *et al.* (1993), respectively.

Sample capsules from completed experiments were embedded in epoxy resin and ground to expose the center of the charges. Most phase compositions were analyzed with an electron microprobe at analytical conditions of 15 kV and 20 nA. Phase X, which was found to be extremely susceptible to beam damage and loss of alkalis, was analyzed with 5 nA beam current and a rastered electron beam as large as the size of phase X grains permitted (typically 10–20 μm). Counting times of 20 s on peaks and 10 s on backgrounds of the X-ray lines were ratioed to a combination of synthetic oxide (Si, Mg, Al), synthetic mineral (Na) and natural mineral (Ca, K) standards. Data were corrected on-line using the PRZ correction procedure. After standardization, no peak search procedures were performed on phase X grains, to minimize residence time of the electron beam. Microprobe analyses of phlogopite and amphibole–pyribole were recalculated assuming stoichiometric OH. No recalculation was attempted for phase X because H_2O was not determined quantitatively.

To search for structural OH in phase X, Raman spectra were recorded at the GL with a Dilor XY confocal micro Raman spectrometer equipped with a cryogenic Wright Model CCD. The excitation source was the 514 nm line of a Coherent Innova Model 90-5 Ar^+ laser operating at 150 mW power using an integration time of 600 s.

PREVIOUS EXPERIMENTAL WORK

Phase X was described as a breakdown product of K-amphibole at P >14 GPa between 1100 and 1400°C in the KCMSH system by Inoue *et al.* (1995*a*, 1998). Luth (1995, 1997) observed phase X in the system phlogopite–diopside at $P \geq 11$ GPa. Based on secondary ionization mass spectrometry (SIMS) measurements of OH combined with microprobe analyses, Inoue *et al.* (1995*a*) proposed a formula of $K_4Mg_8Si_8O_{25}(OH)_2$ for phase X. Experimental results of Luth (1997) and Inoue *et al.* (1998) show a wide range in K_2O contents (10·2–19·4 wt % K_2O) and oxide totals (91·5–98·2 wt %) at relatively constant Si:Mg or Si:(Mg + Al) ratios of 1:1. Phase X may be the 'amphibole-like mineral' reported by Trønnes (1990) as a breakdown product of phlogopite between 11 and 12 GPa. The formula given by Trønnes (1990)—$K_{3·3}Mg_{6·5}Al_{0·5}Si_7O_{22}(OH)_2$—is similar to the composition of phase X reported by Luth (1997) and Inoue et al. (1998).

RESULTS

Petrography and chemical homogeneity of the phases

All starting materials readily recrystallize to mineral grains ~10–50 μm in size at $T \geq 1100$°C and to grains ≤10 μm in size in lower T runs (Fig. 1). HPPs are typically euhedral to subhedral but phase X also forms irregular grains that contain numerous olivine, clinopyroxene, or amphibole inclusions. Many phase X grains show irregularly spaced cleavage (Fig. 1b). A mixed-chain hydrous pyribole (*sensu* Veblen, 1981) was present in three runs, along with K-richterite. The former occurs as lath-shaped to needle-like crystals up to 100 μm × 20 μm in size. In high-P runs, K-hollandite appears as small (≤20 μm × 5 μm) needle-like crystals, and Ca-perovskite forms irregular patches up to 20 μm in size dispersed in the matrix or is present as inclusions in garnet. The phase distribution within individual capsules is inhomogeneous, and melt or quenched fluid is most abundant in the hotter part of the capsule. In experiments on the peralkaline bulk compositions, evidence for quench crystallization is present over a T interval of ≥200°C. The modal amounts of quench vary from <3% at 10 GPa and 1100°C to ~20% at 10 GPa and 1350°C. Near the hot ends of the capsules, along the solid–liquid and quench interface, garnet and clinopyroxene often display larger grain sizes compared with cooler parts of the capsule. Inhomogeneities in grain size and phase distribution can be ascribed to grain maturation and chemical diffusion in a temperature gradient (Lesher & Walker, 1988) aided by the water content of the systems. With the exceptions of large garnets and phase X, neither systematic zoning of individual mineral grains nor differences in phase compositions are observed between tops and bottoms of the capsules. In low-T runs, diffuse Al-rich cores in garnets can be ascribed to incomplete equilibration. Phase X may show strong zoning with respect to K/(K + Na). This

Table 2: Summary of experimental run conditions and run products

Run	Bulk	Assembly	Furnace	*P* (GPa)	*T* (°C)	Run time	Phases observed
Ma88B	per	14/8	LaCr	13·0	1100	07h30	Kr + ga + Mg_2SiO_4 + hiCapx
Ma91B	per	14/8	LaCr	14·0	1100	09h25	Kr + pX + ga + Mg_2SiO_4 + hiCapx
Ma92B	per	14/8	LaCr	15·0	1100	09h40	pX + ga + Mg_2SiO_4 + hiCapx + loCapx
Ma102M	per	14/8	LaCr	18·0	1300	09h45	pX + ga + Mg_2SiO_4 + hiCapx + Q
Ma104M	per	14/8	LaCr	13·0	1400	10h00	ga + hiCapx + Mg_2SiO_4 + Q
JKW7	per	10/5	Re	14·0	1300	07h00	pX + ga + hiCapx + Mg_2SiO_4 + loCapx + Q
JKW9	per	10/5	Re	12·0	1300	06h08	Kr + pX + ga + hiCapx + Mg_2SiO_4 + Q
JKW13	per	10/5	Re	10·0	1200	12h00	Kr + pyr + phl + ga + hiCapx + Mg_2SiO_4 + Q
JKW14	per	10/5	Re	14·0	1200	12h00	Kr + pX + ga + Mg_2SiO_4 + hiCapx + loCapx + Q
JKW15	per	10/5	Re	10·0	1300	48h00	Kr + pyr + phl + ga + hiCapx + Mg_2SiO_4 + Q
JKW16	per	8/3	Re	20·0	1300	07h00	pX + Mg_2SiO_4 + ga + K-holl + Ca-perov
JKW17	per	10/5	Re	11·0	1300	48h00	Kr + hiCapx + ga + Mg_2SiO_4 + Q
JKW18	per	10/5	Re	10·0	1350	08h00	Kr + phl + ga + hiCapx + Mg_2SiO_4 + Q
JKW19	per	10/5	Re	10·0	1100	10h00	Kr + phl + ga + hiCapx + Mg_2SiO_4 + Q
JKW25	per	10/5	Re	15·0	900	36h00	Kr + pX + pyr + hiCapx + loCapx + ga + Mg_2SiO_4
Ma95sB	sub	14/8	LaCr	10·0	1100	10h00	Mg_2SiO_4 + hiCapx + ga + Kr
Ma94sB	sub	14/8	LaCr	15·0	1100	09h48	Mg_2SiO_4 + hiCapx + loCapx + ga + pX
JKW29	sub	10/5	Re	14·0	1100	11h16	Mg_2SiO_4 + hiCapx + ga + pX
JKW41	sub	10/5	Re	13·0	1300	11h45	Mg_2SiO_4 + hiCapx + loCapx + ga + Kr
JKW33	sub	10/5	Re	14·0	1400	12h00	Mg_2SiO_4 + hiCapx + loCapx + ga + pX
JKW34	sub	10/5	Re	14·0	900	48h00	hiCapx + loCapx + ga + phase E + pX
JKW30	sub	10/5	Re	13·0	1100	30h00	Mg_2SiO_4 + hiCapx + loCapx + ga + Kr
JKW47	sub	8/3	Re	20·0	1500	05h00	pX + Mg_2SiO_4 + ga + K-holl + Ca-perov
JKW54	sub	8/3	Re	23·0	1700	03h00	Mg_2SiO_4 + ga + K-holl + Ca-perov + Q
JKW61	sub	8/3	Re	23·0	1500	12h00	Mg_2SiO_4 + ga + K-holl + Ca-perov + Q
JKW64	sub	8/3	Re	20·0	1600	06h00	Mg_2SiO_4 + ga + pX + Ca-perov + Q
JKW66	sub	8/3	Re	14·0	1600	08h00	ga + loCapx + hiCapX + Q
JKW67	sub	8/3	Re	20·0	1800*	03h00	ga + Ca-perov + pX + Q
JKW63	KLB	10/5	Re	12·0	1200	72h00	ga + loCapx + hiCapx + Mg_2SiO_4 + Kr
JKW69	KLB	10/5	Re	14·0	1200	48h00	ga + loCapx + hiCapX + Mg_2SiO_4 + pX
JKW70	KLB	10/5	Re	13·0	1200	72h00	ga + loCapx + hiCapX + ol

Abbreviations of mineral phases are given in Table A1; per, peralkaline KNCMASH system; sub, subalkaline KNCMASH system; KLB = KLB-1 + 10 wt % synthetic K-richterite.
*Capsule slightly off-center, therefore actual *T* was probably not higher than 1700°C.

zoning is fairly regular, with K-rich cores and Na-rich rims, or is patchy and irregular. These compositional inhomogeneities are independent of run duration and temperature.

Phase relations

Peralkaline KNCMASH

In the peralkaline KNCMASH system, HPPs are stable to at least 20 GPa and 1300°C, along with garnet + Mg_2SiO_4 + high-Ca clinopyroxene ± low-Ca clinopyroxene ± K-hollandite ± Ca-perovskite (Fig. 2). With increasing pressure, the first HPP to disappear is phlogopite, which is stable at 10 GPa between 1100°C and 1350°C along with K-richterite, but absent from run JKW17 at 11 GPa and 1300°C. In runs at 11 GPa and 1300°C, and 13 GPa and 1100°C K-richterite is the only stable HPP. At higher pressures, amphibole is joined by phase X as a result of continuous amphibole breakdown. At ≥15 GPa and 1100°C, and 14 GPa and

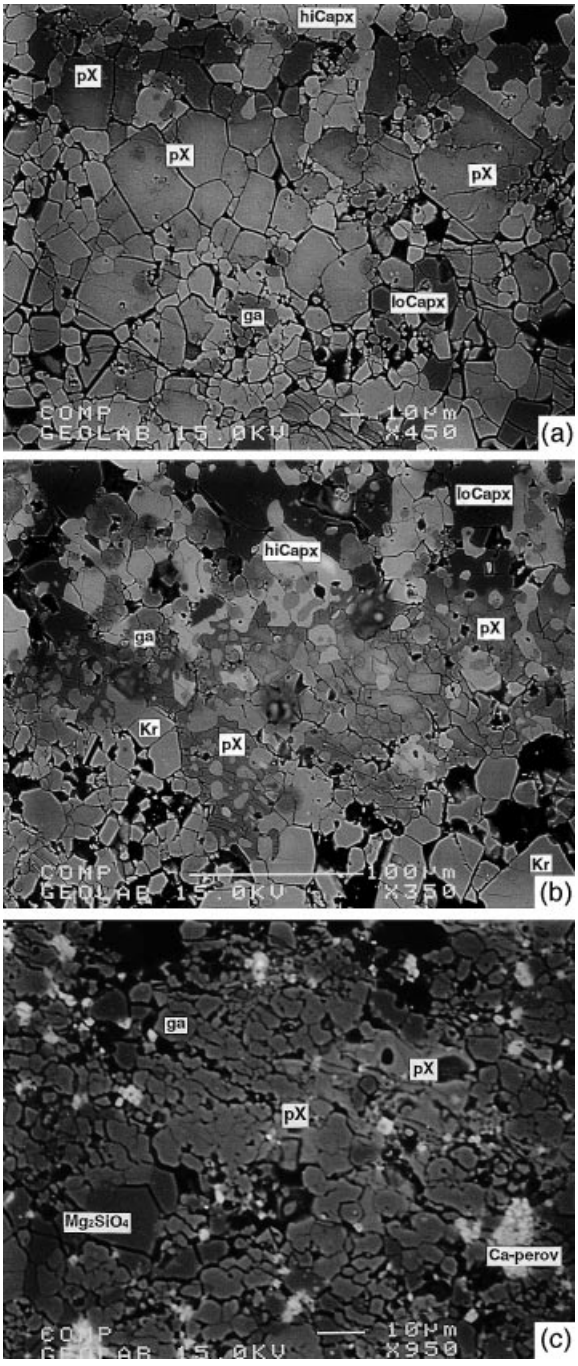

Fig. 1. Back-scattered electron photomicrographs of phase X-bearing assemblages taken from the centers of experimental charges (tops of the images point to the hotter end of the capsules). (a) Run JKW7 at 14 GPa and 1300°C showing euhedral crystals of phase X in part with heterogeneity in K/(K + Na): light areas are K rich, whereas dark areas are more Na rich. (b) Run JKW9 at 12 GPa and 1300°C with coexisting phase X and K-richterite. Phase X shows irregular cleavage and numerous inclusions of Kr and hiCapx. Holes in the sample surface are due to mechanical abrasion during polishing. (c) Run JKW47 at 20 GPa and 1500°C showing poikiloblastic phase X coexisting with majoritic garnet and γ-Mg_2SiO_4; abbreviations are given in Table A1.

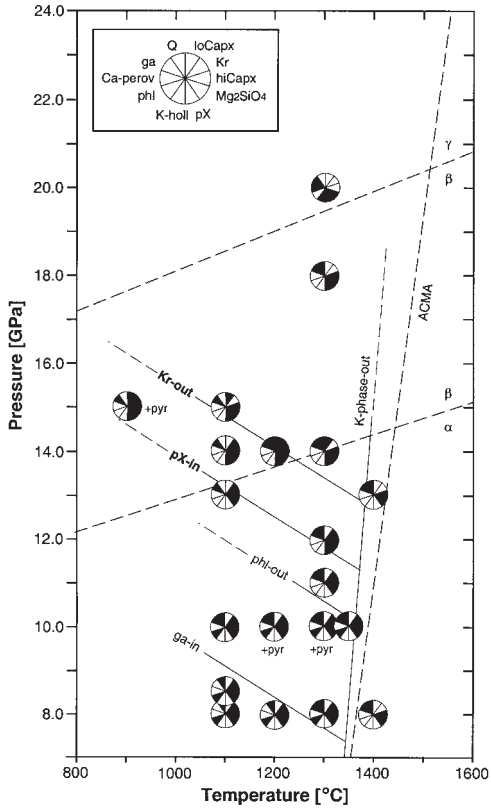

Fig. 2. *P–T* diagram of experimental results in the peralkaline KNCMASH system (Tables 1 and 2). Phases present in the experimental charges are represented by black sectors within the run symbol; phases not detected are denoted by white sectors (inset upper left); abbreviations are given in Table A1; ACMA average current mantle adiabat (see text); α- to β-Mg_2SiO_4 and β- to γ-Mg_2SiO_4 transitions according to Morishima *et al.* (1994) and Katsura & Ito (1989), respectively; experimental data at P <10 GPa from Konzett *et al.* (1997) for comparison.

1300°C, the upper pressure stability limit of K-richterite is reached and amphibole is replaced by phase X as the HPP. Within the spacing of experimental data points, both phase X-in and K-richterite-out reactions have negative slopes with $5\,\text{MPa/K} < \mathrm{d}P/\mathrm{d}T < 15\,\text{MPa/K}$ for phase X-in and $\leq 10\,\text{MPa/K}$ for K-richterite-out. At 20 GPa and 1300°C, K-hollandite appears as the first anhydrous potassic phase as a result of continuous phase X breakdown. Between 18 and 20 GPa, high-Ca clinopyroxene breaks down, and its diopside and jadeite components form Ca-perovskite and sodium-garnet solid solution, respectively.

The high-temperature stability limit of all HPPs is reached between 1300 and 1400°C. At conditions of 8 GPa and 1400°C, and 13 GPa and 1400°C the stable assemblage is garnet + high-Ca clinopyroxene + Mg_2SiO_4 + quench (the term 'quench' is used to denote a mixture of unidentified and mostly K-rich phases that crystallized from a solute-rich fluid or a hydrous melt

upon quenching). The spacing of experimental data points (Fig. 2) precludes discussion of the slope of the K-phase-out reaction(s), but in accordance with results at $P \leq 8{\cdot}5$ GPa (Konzett *et al.*, 1997), we chose a positive slope. Because of the difficulty in distinguishing quenched melts from solute-rich fluids at high pressures based on textural evidence (see Konzett *et al.*, 1997) we did not attempt to locate the position of the solidus. The mixed-chain hydrous pyribole was found in runs at 10 GPa and 15 GPa (Table 3), either with K-richterite + phlogopite or K-richterite alone (see Finger *et al.*, 1998; Konzett & Fei, 1998).

Subalkaline KNCMASH and KLB-1

In the subalkaline system, K-richterite is stable to 13 GPa along with olivine + garnet + high-Ca clinopyroxene ± low-Ca clinopyroxene in an assemblage resembling a metasomatized lherzolite (Fig. 3). The apparent lack of low-Ca clinopyroxene in run Ma95sB is probably due to small grain sizes and the sparse occurrence of this phase in subalkaline runs. At $P \geq 14$ GPa, K-richterite is replaced by phase X. The slope of the K-richterite-out reaction was assumed to be slightly negative, in accordance with the results of K-amphibole breakdown in the KCMSH system obtained by Inoue *et al.* (1998). Phase X is stable to at least 20 GPa. At this pressure, phase X may coexist with K-hollandite as a result of H_2O partitioning constraints (see below), and with Ca-perovskite produced by the breakdown of high-Ca clinopyroxene. At 23 GPa, phase X is absent and K-hollandite carries the K in the system. The upper T stability limit of phase X is between 1400 and 1600°C at 14 GPa, in an assemblage without a solid K-rich phase: high-Ca clinopyroxene + garnet + low-Ca clinopyroxene + quench. At 20 GPa, the K-phase-out reaction must occur at $T > 1700$°C, which is at least 200°C above an average current mantle adiabat (ACMA) as defined by a $\beta \rightarrow \gamma$ transition in Mg_2SiO_4 at 17·9 GPa and 1475°C (Katsura & Ito, 1989) and a $\gamma \rightarrow$ perovskite + wüstite transition at 23·2 GPa and 1530°C (Ito & Takahashi, 1989).

In the K-richterite-doped peridotite KLB-1, HPPs coexist with garnet + low-Ca clinopyroxene + high-Ca clinopyroxene + Mg_2SiO_4. K-richterite is stable at 12 GPa and 1200°C after a run duration of 72 h. X-ray mapping also showed that a K-rich phase is dispersed within graphite, along the interface between experimental charge and inner graphite capsule (see Konzett & Ulmer, 1999). At 13 GPa and 1200°C, after an identical run time, no HPP could be identified and X-ray mapping showed that all K was concentrated at the charge–graphite interface in diffuse grain boundary films. Because of their extremely small grain size, the K-carrying phase(s) could not be identified. Small amounts of alkaline and possibly CO_2-rich fluid that probably formed by amphibole breakdown and/or graphite oxidation evidently destabilized phase X with increasing run durations. In a run that lasted only 48 h, phase X was stabilized at 14 GPa and 1200°C (see Table 9, below). Thus, the amphibole breakdown for starting material KLB-1 was placed between 12 and 13 GPa at 1200°C, which is 1 GPa below the amphibole → phase X transition in the subalkaline KNCMASH system (Fig. 3).

Mineral chemistry

K-amphibole and hydrous pyribole

In both peralkaline and subalkaline systems, the K-rich amphibole is K-richterite (Leake, 1978; revised Leake *et al.*, 1997), which increases in K per formula unit (p.f.u.) and K/(K + Na) with P (Table 3, Fig. 4), as shown by Konzett *et al.* (1997). Above 8 GPa, amphibole has K in the M(4) site, with a maximum K(M4) of 0·51 ± 0·02 at 13 GPa and 1300°C in the subalkaline system. In the peralkaline system, K-richterite is the only HPP at 13 GPa and 1100°C and, hence, the K contents of amphibole depend only upon the bulk K contents. The lack of coexisting HPP can explain the sudden increase in K p.f.u. of amphibole and the deviation from the almost linear K p.f.u.–P trend (Fig. 4). In the subalkaline system, K-richterite is the only K phase at $P \geq 9$ GPa, and therefore the increase in K p.f.u. and K/(K + Na) must be compensated by a decrease in the modal amount of amphibole within that P range (assuming constant or increasing K in the fluid phase). The amphibole contains small amounts of Al both as Al(IV) and Al(VI), and Al_{tot} decreases with increasing P to 0·09 and 0·12 p.f.u. in the subalkaline and peralkaline systems, respectively (Fig. 4). The Tschermak component decreases with increasing P, but it is sensitive to changes in the coexisting Mg-phase assemblage. This may explain the reversals in the observed Al(VI)–P trend (e.g. phl-out at >10 GPa and >8 GPa in the peralkaline and subalkaline systems). The decrease of the Tschermak (tk) component can be attributed to a model reaction

$$4 \text{ tremolite} + 4 \text{ olivine} + 5 \text{ tk} = 8 \text{ diopside} + 5 \text{ pyrope} + 4\ H_2O \quad (1)$$

$$4\ Ca_2Mg_5Si_8O_{22}(OH)_2 + 4\ Mg_2SiO_4 + 5\ Al_2Mg_{-1}Si_{-1} = 8\ CaMgSi_2O_6 + 5\ Mg_3Al_2Si_3O_{12} + 4\ H_2O \quad (1a)$$

in which garnet and high-Ca clinopyroxene grow at the expense of amphibole. Reaction (1) is equivalent to a reaction

$$4 \text{ tremolite} + 3 \text{ tk} = 8 \text{ diopside} + 3 \text{ pyrope} + 4 \text{ quartz} + 4\ H_2O$$

which buffers the Tschermak content of calcic amphibole in tonalitic systems below the albite + quartz = jadeite reaction (Schmidt, 1993).

Table 3: Average analyses of K-richterite and mixed-chain hydrous pyribole

Exp.:	JKW19	JKW13		JKW15		JKW18	JKW17	JKW9	Ma88sB	Ma91B	JKW14	JKW25	Ma95sB	JKW30	JKW41	
Bulk:	per	per		per		per	per	per	per	per	per	per		sub	sub	sub
P (GPa):	10	10		10		10	11	12	13	14	14	15		10	13	13
T (°C):	1100	1200		1300		1350	1300	1300	1100	1100	1200	900		1100	1100	1300
	amph	amph	pyr	amph	pyr	amph	amph	amph	amph	amph	amph	amph	pyr	amph	amph	amph
No. of analyses:	9	10	6	10	13	6	13	9	7	9	6	3	8	8	5	6
SiO_2	56·1(2)	55·0(2)	56·4(3)	55·8(4)	57·2(2)	54·5(5)	55·9(3)	55·9(4)	57·1(3)	57·5(6)	56·9(4)	56·4(6)	57·2(4)	56·4(1)	56·8(6)	56·4(3)
Al_2O_3	2·8(1)	2·9(2)	5·2(3)	2·5(1)	5·2(3)	3·5(1)	3·0(2)	1·7(2)	0·8(1)	0·6(0)	0·5(1)	0·3(3)	3·3(3)	1·0(1)	0·5(5)	0·7(0)
MgO	23·7(1)	23·0(2)	18·8(2)	23·1(2)	18·4(3)	22·8(3)	23·0(3)	23·1(3)	24·2(2)	24·0(1)	23·7(1)	23·7(3)	20·2(8)	24·2(1)	23·9(4)	23·5(2)
CaO	7·1(2)	6·7(4)	8·2(3)	6·6(2)	7·6(4)	7·0(2)	6·2(4)	6·1(3)	6·3(2)	6·2(1)	6·4(2)	6·3(3)	9·5(4)	6·8(1)	6·2(1)	5·8(1)
Na_2O	3·1(1)	2·9(2)	5·0(2)	2·8(2)	5·3(3)	2·7(1)	2·7(3)	2·5(2)	2·6(1)	2·9(1)	2·8(2)	2·9(1)	4·2(3)	2·4(1)	2·4(1)	2·1(1)
K_2O	6·3(1)	6·8(2)	4·4(1)	6·8(1)	4·3(0)	6·8(1)	7·5(1)	7·7(1)	7·6(2)	7·1(1)	7·3(1)	7·5(1)	4·3(2)	7·3(2)	7·8(2)	8·4(1)
H_2O	2·2(0)	2·1(0)	1·4(0)	2·2(0)	1·4(0)	2·1(0)	2·2(0)	2·1(0)	2·2(0)	2·2(0)	2·1(0)	2·1(0)	1·4(0)	2·2(0)	2·1(0)	2·1(0)
Σ	101·2(5)	99·3(3)	99·4(4)	99·8(6)	99·4(3)	99·4(7)	100·5(3)	99·1(5)	100·7(5)	100·7(7)	99·6(4)	99·4(1)	100·2(8)	100·2(2)	99·8(8)	99·1(5)
Si	7·73(1)	7·73(1)	11·86(2)	7·79(2)	11·98(2)	7·66(3)	7·77(3)	7·89(1)	7·93(1)	7·96(2)	7·98(2)	7·95(1)	11·97(3)	7·87(1)	7·96(2)	7·98(1)
Al	0·45(1)	0·48(3)	1·29(6)	0·41(1)	1·29(8)	0·58(2)	0·49(4)	0·29(3)	0·13(1)	0·12(1)	0·08(1)	0·05(1)	0·80(7)	0·17(1)	0·10(1)	0·12(0)
Mg	4·86(1)	4·81(4)	5·90(6)	4·81(3)	5·74(9)	4·79(1)	4·77(6)	4·85(4)	5·00(3)	4·95(0)	4·95(4)	4·98(2)	6·30(2)	5·03(2)	5·00(6)	4·94(2)
Ca	1·05(2)	1·01(5)	1·84(7)	0·99(3)	1·71(8)	1·06(3)	0·93(6)	0·92(4)	0·93(1)	0·92(1)	0·96(3)	0·96(4)	2·13(9)	1·01(1)	0·92(2)	0·88(1)
Na	0·84(3)	0·78(6)	2·04(7)	0·76(5)	2·14(9)	0·73(3)	0·73(7)	0·68(5)	0·69(2)	0·78(2)	0·75(5)	0·80(1)	1·69(1)	0·64(3)	0·65(4)	0·57(1)
K	1·19(1)	1·21(3)	1·19(2)	1·22(2)	1·15(1)	1·22(3)	1·33(2)	1·39(3)	1·34(3)	1·26(1)	1·30(2)	1·35(1)	1·16(5)	1·30(3)	1·40(4)	1·52(3)
Σ	16·02(2)	16·02(1)	24·11(1)	15·99(2)	24·01(4)	16·02(2)	16·02(1)	16·01(3)	16·02(1)	16·01(1)	16·01(3)	16·10(1)	24·05(3)	16·02(1)	16·02(4)	16·01(2)
K/(K+Na)	0·57(1)	0·61(2)	0·37(1)	0·62(2)	0·35(1)	0·63(2)	0·65(2)	0·67(2)	0·66(1)	0·62(1)	0·64(2)	0·58(1)	0·41(2)	0·67(1)	0·68(1)	0·73(1)

Amphibole formulae recalculated to 23 oxygens + stoichiometric OH; pyribole formulae recalculated to 33 oxygens + stoichiometric OH; numbers in parentheses denote 1σ SD.

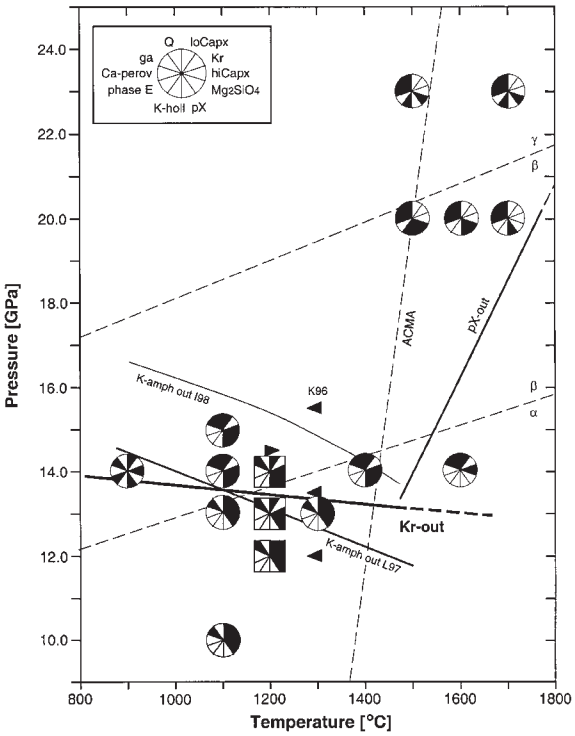

Fig. 3. *P–T* diagram of experimental results in the subalkaline KNCMASH (pie symbols) and the KLB-1 (square symbols) systems (Tables 1 and 2). Meaning of symbols, ACMA and $\alpha \rightarrow \beta \rightarrow \gamma$ transitions in Mg_2SiO_4 as in Fig. 2; K-amph out I98 and L97 indicate K-amphibole-out reactions in the KCMSH and KCMASH systems according to Inoue *et al.* (1998) and Luth (1997), respectively; filled arrows bracket position of H_2O-saturated solidus for KLB-1 peridotite according to Kawamoto *et al.* (1996) (K96).

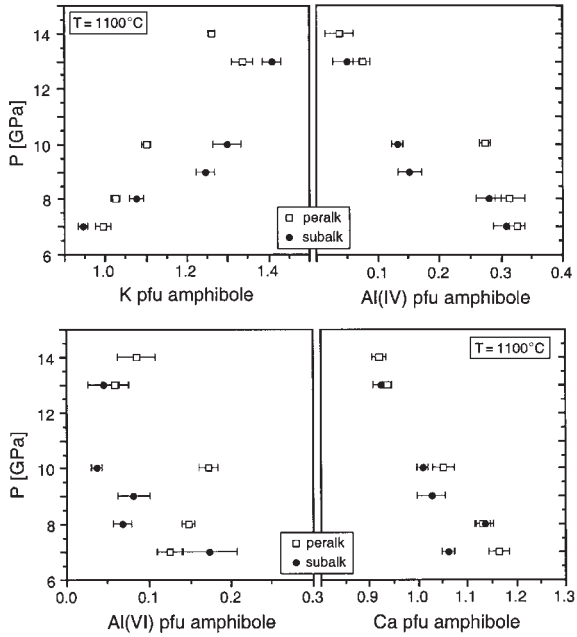

Fig. 4. Selected mineral chemical parameters of K-richterite as a function of *P* at constant *T* (1100°C) for peralkaline and subalkaline KNCMASH systems; each point represents an average of 5–13 individual amphibole analyses (Table 3).

In the KLB-1 starting composition, amphibole at its upper *P* stability limit is still close to K-richterite end-member composition (see Table 9, below) with 1·07–1·13 K p.f.u. and 0·11–0·13 Al p.f.u. The X_{Mg} for amphibole is 0·95 with $X_{Mg}^{Kr} > X_{Mg}^{loCapx} > X_{Mg}^{ol} > X_{Mg}^{hiCapx} > X_{Mg}^{ga}$.

A mixed-chain hydrous pyribole (Thompson, 1981; Veblen, 1981) was found with K-richterite ± phase X at 10 and 15 GPa. According to Finger *et al.* (1998), the pyribole belongs to the $M_nPM(n-1)P$ series with $n = 1$ and contains alternating single and double tetrahedral chains. The pyribole is a combination of 2 omphacite + 1 K-richterite, which ideally would yield

$$KNaCaMg_5Si_8O_{22}(OH)_2 + 2\ Ca_{0.5}Na_{0.5}Mg_{0.5}Al_{0.5}Si_2O_6 = KNa_2Ca_2Mg_6AlSi_{12}O_{34}(OH)_2. \quad (2)$$

Pyribole compositions at 10 GPa are slightly enriched in Na and Al(VI) and depleted in Mg and Ca (Fig. 5), which can be explained by combined Tschermak and plagioclase exchange

$$KNa_2Ca_2Mg_6AlSi_{12}O_{34}(OH)_2 + Al_2Mg_{-1}Si_{-1} + NaSiCa_{-1}Al_{-1} = KNa_3CaMg_5Al_2Si_{12}O_{34}(OH)_2 \quad (3)$$

operating on the pyroxene-layers within the pyribole structure. Pyribole formed at 15 GPa is poorer in Al and Na and richer in Ca and Mg relative to the ideal 2 omphacite + K-richterite combination, indicating the operation of reaction (3) in the opposite direction, which shifts the composition towards the hypothetical end-member $KNaCa_3Mg_7Si_{12}O_{34}(OH)_2$ (Fig. 5). These compositional changes can be rationalized in terms of the end-member reactions

$$KNaCaMg_5Si_8O_{22}(OH)_2 + 2\ NaAlSi_2O_6 = KNa_3CaMg_5Al_2Si_{12}O_{34}(OH)_2 \quad (4a)$$

$$KNaCaMg_5Si_8O_{22}(OH)_2 + 2\ CaMgSi_2O_6 = KNaCa_3Mg_7Si_{12}O_{34}(OH)_2 \quad (4b)$$

each involving K-richterite and a clinopyroxene end-member. The decrease in Al and increase in K/(K + Na) (Table 3) with increasing *P* is consistent with the behaviour of K-richterite, phase X (see below) and phlogopite (Konzett *et al.*, 1997).

Phlogopite

Phlogopite is near the end-member composition, with a small excess of 0·02–0·04 Si p.f.u. (Table 4), indicating limited solid-solution with $K(Mg_{2.5}\square_{0.5})Si_4O_{10}(OH)_2$ (Seifert & Schreyer, 1971).

Phase X

Phase X is a disilicate (Libau, 1982), containing corner-sharing SiO_4 tetrahedra and has a stoichiometry A_{2-}

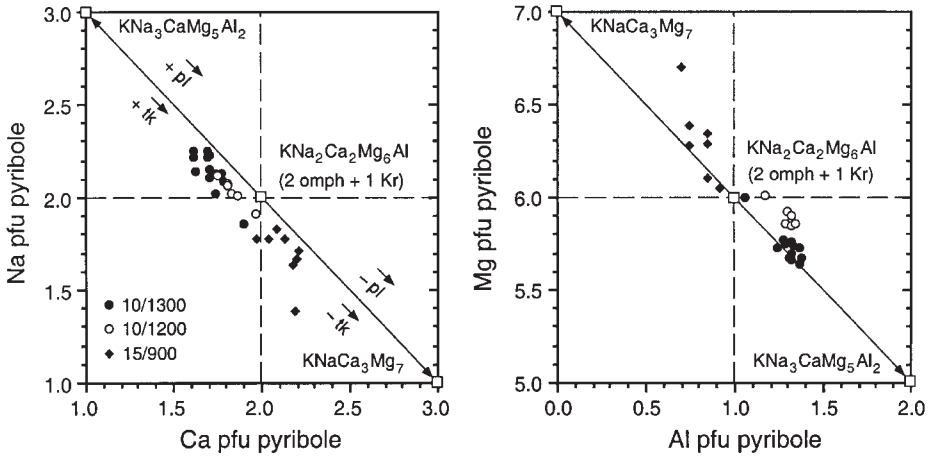

Fig. 5. Compositional variation of mixed-chain hydrous pyribole in terms of Na–Ca and Mg–Al; □, hypothetical pyribole end-member compositions (see text for explanation).

Table 4: Average analyses of phlogopite

Exp.:	JKW19	JKW13	JKW15	JKW18
P (GPa):	10	10	10	10
T (°C):	1100	1200	1300	1350
No. of analyses:	8	5	10	7
SiO_2	43·9(2)	43·6(1)	43·3(4)	43·4(4)
Al_2O_3	11·8(1)	11·5(1)	11·8(2)	11·6(2)
MgO	28·9(2)	28·5(2)	28·7(1)	28·2(2)
CaO	<0·05	<0·05	<0·05	<0·05
Na_2O	0·1(1)	0·1(0)	0·1(0)	0·2(0)
K_2O	11·4(1)	11·4(1)	11·2(1)	11·4(2)
H_2O	4·3(0)	4·3(0)	4·3(0)	4·3(0)
Σ	100·4(5)	99·5(4)	99·4(6)	99·0(7)
Si	3·04(1)	3·04(1)	3·02(1)	3·04(2)
Al	0·96(0)	0·95(1)	0·97(1)	0·96(1)
Mg	2·98(2)	2·97(1)	2·99(2)	2·95(2)
Ca	—	—	—	—
Na	0·01(1)	0·01(0)	0·01(0)	0·02(1)
K	1·00(1)	1·00(1)	1·00(1)	1·02(2)
Σ	7·99(1)	8·00(1)	7·99(1)	7·99(1)
K/(K+Na)	0·99(1)	0·99(0)	0·99(0)	0·98(0)

Phlogopite formulae recalculated to 11 oxygens + stoichiometric OH.

$xB_2Si_2O_7H_x$ with A = K or Na, B = Mg, Al or Ca, and x = 0–1, ranging from anhydrous $A_2B_2Si_2O_7$ to $A□B_2Si_2O_7H$ with a maximum possible H_2O content of 3·51 wt % and a vacancy on the A-position (H. Yang & J. Konzett, unpublished data, 1999; Konzett & Yang, 1998). Variable H_2O contents have been observed in phase E (Kudoh *et al.*, 1993), phase D (Frost & Fei, 1998), hydrous wadsleyite (Kudoh *et al.*, 1996) or hydrous modified spinel (Inoue *et al.*, 1995*b*). The presence of OH in phase X in both subalkaline and peralkaline systems was confirmed by laser Raman spectroscopy. Raman spectra show strong peaks in the OH-stretching region at 3600 cm^{-1} (Fig. 6). This is consistent with low average analytical oxide totals in the range of 96–98 wt % in most runs (Table 5). In the silicate stretching region, phase X spectra are characterized by major peaks at 635–640 cm^{-1} and 895–903 cm^{-1} (Fig. 6). The composition of phase X may be inhomogeneous in K/(K + Na), which may range between 0·15 and 0·88 in an individual run (Table 5). This compositional inhomogeneity is restricted to the K/(K + Na) ratio and occurs even if the coexisting phases are well equilibrated. Other chemical characteristics such as Al or Ca contents and Mg/Si ratios show no correlation with K/(K + Na). A decrease in the degree of inhomogeneity can be observed with increasing pressure and K_2O contents. Because the inhomogeneity of the phase X composition is independent of run duration and temperature, it cannot be easily explained by a failure of the runs to attain equilibrium. It might instead be a quench effect promoted by high Na contents of phase X. This effect may result from the difference of the ionic radii of K and Na, which leads to a lattice collapse during pressure release. Excluding Na-rich rims, an increase in K_2O and a decrease in Na_2O with increasing P (and T) is observed (Fig. 7). In the subalkaline bulk composition, the highest K_2O contents of phase X (20–25 wt %) are correlated with the highest oxide totals of >99 wt % (Fig. 8). Although oxide totals can be affected by the analytical technique (i.e. variable electron beam raster size adjusted

to grain size of phase X) this correlation indicates decreasing H_2O contents of phase X with increasing *P*. The effect may be explained by an increasing ability of coexisting phases—especially Mg_2SiO_4—to incorporate H_2O (Kohlstedt *et al.*, 1996), which changes H_2O partitioning and leads to a continuous dehydration of phase X. The increase in K of phase X with pressure is consistent with other studies (Luth, 1997; Inoue *et al.*, 1998) and parallels results for phlogopite and K-richterite (Konzett & Ulmer, 1999).

Phase X contains from 0·4 to 2·6 wt % Al_2O_3 and from 0·05 to 0·5 wt % CaO, respectively, values consistent with observations by Luth (1997) and Inoue *et al.* (1998). Al decreases with increasing *P* at constant *T*, but varies little with *T* (Fig. 7). The increase of Al in phase X in the peralkaline bulk composition at 20 GPa reflects the stabilization of K-hollandite. The molar Si/(Mg + Al) ratios of individual phase X analyses are consistently closer to 1·0 than are the Si/Mg ratios. This suggests a replacement of six-coordinated Mg by Al through a coupled substitution to maintain charge balance. Although there are several possibilities, such as $\square Al_2Mg_{-3}$ or $AlAlMg_{-1}Si_{-1}$, the structure analysis gives no indication of $^{[IV]}Al$ and the most likely substitution is $Al\square Mg_{-1}K_{-1}$. This exchange introduces a further vacancy on the K position for charge balance and would lead to a theoretical phase X end-member $\square_2(MgAl)Si_2O_7H$ or $\square K(MgAl)Si_2O_7$ for the anhydrous end-member. The Ca content of phase X does not exceed 0·8 wt % (Fig. 7) and can be explained by a simple $CaMg_{-1}$ exchange.

Garnet

All synthesized garnets are Mg-rich pyrope–grossular solid solutions with $X_{Ca} \leq 0{\cdot}45$ (Table 6). Garnet analyses consistently show >3 Si p.f.u., indicating the presence of a majorite component as a result of $Mg_3Al_2Si_3O_{12} + MgSiAl_{-2} = Mg_3[MgSi]Si_3O_{12}$. The amount of majorite component increases with *P* and *T*, consistent with results of previous studies (e.g. Ringwood, 1967; Kanzaki, 1987; Luth, 1997). A small amount of excess Si is also introduced through a Na-garnet component as a result of a continuous reaction

$$(Ca,Mg)_3Al_2Si_3O_{12} + NaSi(Ca,Mg)_{-1}Al_{-1} = Na(Ca,Mg)_2[AlSi]Si_3O_{12} \quad (5)$$

(Ringwood & Major, 1971; Irifune *et al.*, 1994). Na increases with increasing *P* (Fig. 9) and above the upper *P* stability limit of high-Ca clinopyroxene at >18 GPa (Oguri *et al.*, 1997), garnet represents the major subsolidus host for Na as a result of a reaction of jadeite component (see Gasparik, 1989)

$$NaAlSi_2O_6 + Mg_2Si_2O_6 = NaMg_2[SiAl]Si_3O_{12}. \quad (6)$$

The reason for the anomalously high Na in garnets from JKW47 is not clear; it might be due to incomplete equilibration. Potassium contents of garnet are <800 ppm at pressures up to 23 GPa.

High-Ca clinopyroxene

High-Ca clinopyroxene is essentially a binary diopside–jadeite solid solution with <0·25 Na p.f.u. and minor amounts of Mg(M2) in most cases (Table 7). Na varies little between 10 and 15 GPa but decreases strongly near the upper *P* stability limit of clinopyroxene to 0·06 Na p.f.u., equivalent to 5 mol % jadeite component. This reflects a continuous reaction of jadeite component to form Na-garnet (see above). Averaged K contents range between 0·2 and 0·8 wt % K_2O. These lack systematic trends with either *P* or *T*, instead reflecting the strong dependence of K in high-Ca clinopyroxene upon the coexisting assemblage (Luth, 1997).

K-hollandite and Ca-perovskite

K-hollandite is close to stoichiometric $KAlSi_3O_8$ with K p.f.u. of 0·97–0·99 and small amounts of Mg and Ca (Table 8). Ca-perovskite is close to $CaSiO_3$ with negligible $MgSiO_3$ component. All analyzed Ca-perovskites contain 0·3–5·5 wt % Al_2O_3, 0–0·4 wt % Na_2O and 0·4–1·0 wt % K_2O (Table 8). In the absence of Fe^{3+}, possible mechanisms for incorporation of Al into the Ca-perovskite structure are $^{[XII]}Al^{[VI]}Al^{[XII]}Ca_{-1}{}^{[VI]}Si_{-1}$ (Andrault *et al.*, 1998) or $^{[XII]}Al^{[XII]}Na^{[XII]}Ca_{-2}$ (Kesson *et al.*, 1995). The small number of analyses and the relatively large scatter of the data do not allow us to assess whether or not K can enter the perovskite structure.

DISCUSSION

K-amphibole breakdown

Experiments in natural KLB-1 and in the KNCMASH system indicate an upper *P* stability limit of K-amphibole at 12–14 GPa, corresponding to 340–400 km depth. In the KLB-1 system, amphibole is close to pure K-richterite with only minor K on M(4) even at its upper *P* stability limit (Table 9). Assuming $KNaCaMg_5Si_8O_{22}(OH)_2$ and $KHMg_2Si_2O_7$ as amphibole and phase X compositions, continuous reactions that produce phase X from K-amphibole breakdown can be written as

$$\text{amphibole} + \text{garnet} = \text{high-Ca clinopyroxene} + \text{low-Ca clinopyroxene} + \text{phase X} + H_2O \quad (7a)$$

$$\text{amphibole} + \text{garnet}_1 = \text{garnet}_2 + \text{high-Ca clinopyroxene} \pm \text{low-Ca clinopyroxene} + \text{phase X} + H_2O \quad (8a)$$

with model end-member reactions

Table 5: Average and representative analyses of phase X

Exp.:	JKW9		Ma91B		JKW14		JKW7		JKW25	Ma92B		Ma102M	JKW16	Ma94sB	JKW29	JKW64	JKW67
P (GPa):	12		14		14		14		15	15		18	20	15	14	20	20
T (°C):	1300		1100		1200		1300		900	1100		1300	1300	1100	1100	1600	1800
Bulk:	per		per		per		per		per	per		per	sub	sub	sub	sub	sub
	K-rich	Na-rich	K-rich	Na-rich	K-rich	Na-rich	K-rich	Na-rich		K-rich	Na-rich						
No. of analyses:	6	6	11	11	3	3	7	7	7	9		7	16	15	5	5	3
SiO_2	47·2(7)	46·0	48·3(1)	49·8	46·3(5)	47·8	45·7(5)	44·7	44·1(9)	47·6(8)	51·1	47·9(8)	47·7(6)	47·8(8)	46·4(1)	45·8(8)	43·7(9)
Al_2O_3	2·5(1)	2·6	2·1(0)	2·3	2·1(1)	2·3	1·9(1)	1·9	2·1(3)	2·2(2)	2·2	1·4(0)	2·1(3)	2·0(2)	1·9(1)	1·2(1)	0·6(1)
MgO	29·3(4)	28·7	30·4(6)	31·8	29·5(3)	31·7	30·3(4)	28·9	28·1(5)	30·9(6)	33·1	31·2(5)	30·4(7)	31·1(4)	30·3(6)	29·8(6)	29·4(3)
CaO	0·2(0)	0·2	0·2(0)	0·2	0·3(0)	0·4	0·3(1)	0·3	0·3(2)	0·2(1)	0·3	0·5(1)	0·5(1)	0·3(1)	0·2(0)	0·4(0)	0·2(1)
Na_2O	3·8(3)	7·6	1·7(2)	7·3	2·3(1)	11·4	2·3(3)	3·5	1·1(5)	2·0(3)	7·7	1·8(3)	1·1(3)	2·3(4)	2·0(2)	1·5(2)	1·7(0)
K_2O	14·1(1)	11·2	15·1(6)	2·4	16·9(4)	3·8	17·8(9)	17·6	22·8(1)	15·7(5)	2·9	16·3(6)	17·4(5)	14·5(6)	16·3(1)	20·8(7)	25·0(7)
Σ	97·0(7)	96·2	97·9(1)	93·8	97·3(7)	97·3	98·2(1)	96·9	98·5(9)	98·5(1)	97·4	99·1(1)	99·2(7)	98·0(7)	96·8(1)	99·3(7)	100·5(5)

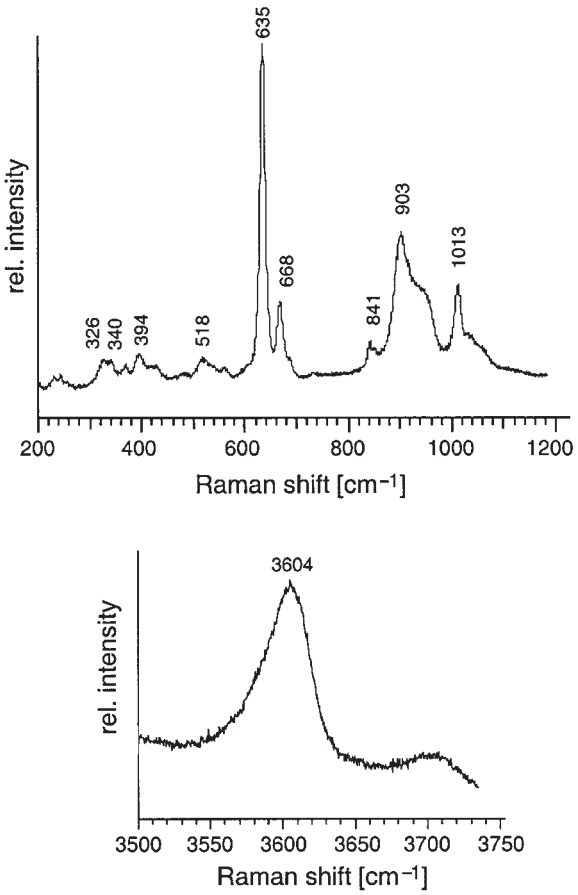

Fig. 6. Unoriented laser Raman spectrum of phase X from run JKW7 (14 GPa and 1300°C, peralkaline KNCMASH) in the silicate (200–1200 cm^{-1}) and the OH-stretching region (3500–3750 cm^{-1}).

$$4\ \mathrm{Kr} + 2\ \mathrm{gross} = 4\ \mathrm{jad} + 10\ \mathrm{di} + \mathrm{cen} + 4\ \mathrm{pX} + 2\ \mathrm{H_2O} \quad (7b)$$

$$4\ \mathrm{Kr} + 2\ \mathrm{py} = 4\ \mathrm{jad} + 4\ \mathrm{di} + 7\ \mathrm{cen} + 4\ \mathrm{pX} + 2\ \mathrm{H_2O} \quad (7c)$$

$$12\ \mathrm{Kr} + 7\ \mathrm{gross} = 12\ \mathrm{jad} + 33\ \mathrm{di} + \mathrm{py} + 12\ \mathrm{pX} + 6\ \mathrm{H_2O} \quad (8b)$$

$$12\ \mathrm{Kr} + 10\ \mathrm{py} = 12\ \mathrm{jad} + 33\ \mathrm{cen} + 4\ \mathrm{gross} + 12\ \mathrm{pX} + 6\ \mathrm{H_2O}. \quad (8c)$$

These reactions involve a continuous change in garnet composition as a result of CaMg exchange and limited $MgSiO_3$ solubility to form majorite component in garnet. The small amounts of Na in phase X can be ascribed to reactions forming $NaHMg_2Si_2O_7$ component instead of jadeite component in clinopyroxene. Reactions involving $NaHMg_2Si_2O_7$ component can be written as

$$\text{amphibole} + \mathrm{Mg_2SiO_4} + \mathrm{garnet_1} = \mathrm{garnet_2} + \text{high-Ca clinopyroxene} + \text{low-Ca clinopyroxene} + \text{phase X} \quad (9)$$

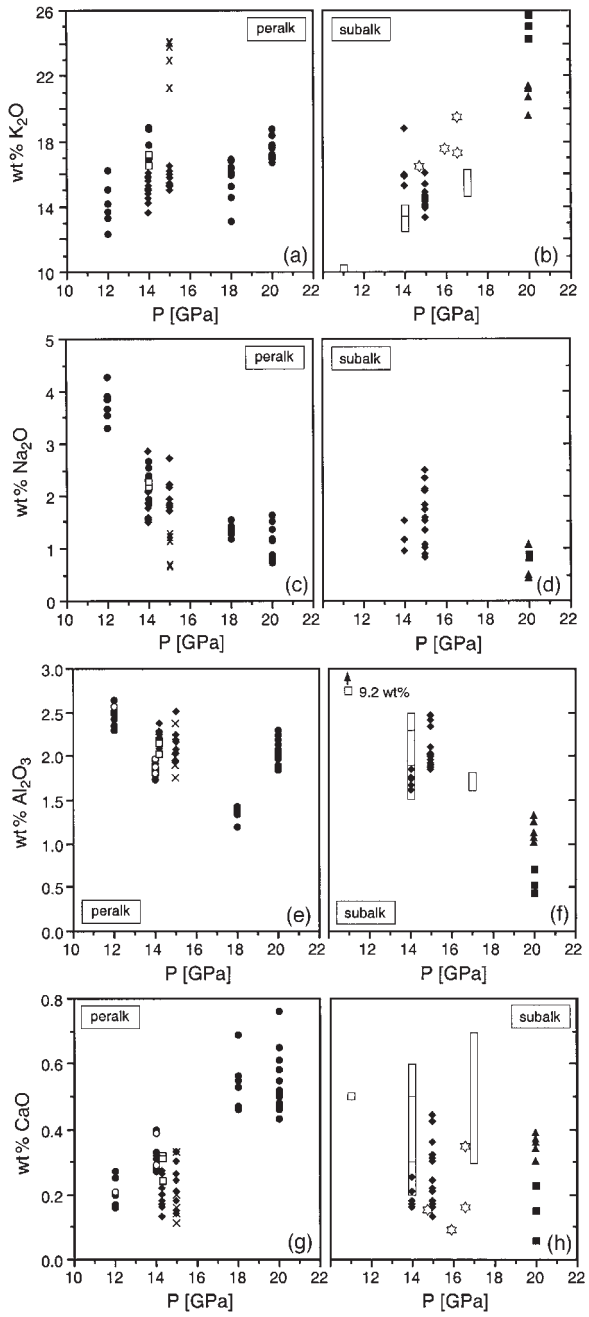

Fig. 7. Selected mineral chemical parameters of phase X as a function of *P* and *T*. ●, Runs at 1300°C; ◆, runs at 1100°C; □, runs at 1200°C; ×, runs at 900°C; ■, runs at 1700°C; ▲, runs at 1600°C; open bars, composition range of phase X (Luth,1997); open stars, compositions of phase X obtained by Inoue *et al.* (1998); in (e) and (g), ○ and ● are analyses of K-rich and Na-rich grains/grain areas of phase X (see Table 5), respectively; in (a) and (c), only K-rich phase X analyses are plotted.

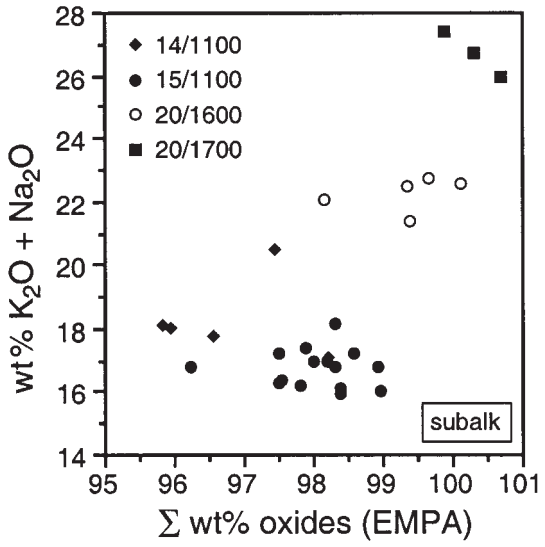

Fig. 8. Plot of wt % (K_2O + Na_2O) vs oxide totals obtained from electron microprobe analyses for phase X from the subalkaline KNCMASH system. Only K-rich phase X analyses are plotted.

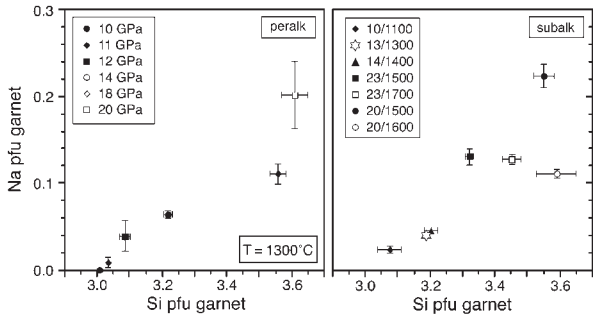

Fig. 9. Plot of Na p.f.u. vs Si p.f.u. for garnets from the subalkaline and peralkaline KNCMASH systems.

$$3\ \mathrm{Kr} + 6\ \mathrm{Mg_2SiO_4} + \mathrm{py} = 9\ \mathrm{cen} + \mathrm{gross} + 3\ \mathrm{pX} + 3\ \mathrm{NapX} \quad (9b)$$

$$3\ \mathrm{Kr} + 6\ \mathrm{Mg_2SiO_4} + 2\ \mathrm{gross} = 9\ \mathrm{di} + 2\ \mathrm{py} + 3\ \mathrm{pX} + 3\ \mathrm{NapX}. \quad (9c)$$

Reaction (9) has olivine as an additional reactant, which will shift the reaction to lower P and T compared with reactions (7) and (8). Initial amphibole breakdown to an $NaHMg_2Si_2O_7$ component would be consistent with the fact that phase X is richest in Na at the lowest P at which phase X is stable. Reactions (7) and (8) produce free fluid because the K/H ratio of phase X is higher than that of amphibole. The amount of water produced per mol of amphibole consumed increases for phase X compositions with decreasing H content. Analytical totals of microprobe analyses suggest that phase X contains less than the theoretical maximum amount of H. This is supported by SIMS analyses of phase X by Inoue *et al.* (1998), which yielded 1·7 ± 0·1 wt % H_2O, equivalent to $K_{1\cdot5}Mg_2Si_2O_7H_{0\cdot5}$. Moreover, because of the possibility of electron beam damage and alkali diffusion, water contents inferred from microprobe analytical totals are maximum values. Analyses of phase X grains formed at 20 GPa yield the highest K_2O values and display analytical totals indistinguishable from 100 wt %. This suggests that H_2O decreases in phase X with increasing P, which could be explained by changing H_2O partitioning with coexisting nominally anhydrous phases, especially Mg_2SiO_4 high-pressure polymorphs and melts or fluids. P–T dependent variations in the H_2O contents of phase D were inferred on the basis of variable analytical oxide totals by Frost & Fei (1998) and may also be present in phase E (Kudoh *et al.*, 1993), hydrous wadsleyite (Kudoh *et al.*, 1996), and hydrous spinel (Inoue *et al.*, 1995*b*). The importance of H_2O partitioning for the phase relations is illustrated by comparing data for runs JKW47 and JKW64 at 20 GPa and 1500 and 1600°C. In JKW47, phase X coexists with K-hollandite + ~20 vol. % Mg_2SiO_4. In JKW64, phase X is the only K phase, and it coexists with <5 vol. % Mg_2SiO_4. Because of the much larger amount of Mg_2SiO_4 present in JKW47 compared with JKW64 (and assuming constant, $D_{H_2O}^{Mg_2SiO_4\text{–phase X}}$), too little H_2O is available to form phase X, and an additional anhydrous K phase—K-hollandite—forms.

In the KLB-1 bulk composition K-amphibole breaks down between 12 and 13 GPa at 1200°C, equivalent to depths of 360–390 km. Within this depth interval, the α to α + β transition occurs for olivine (Fo_{90}) (Katsura & Ito 1989). Because of the high solubility of H_2O in Mg_2SiO_4 (0·1–0·15 wt % in ol at 10–13 GPa; 2·1–2·4 wt % in β-Mg_2SiO_4 at 14–15 GPa; Young *et al.*, 1993; Kohlstedt *et al.*, 1996), the generation of a free H_2O fluid from K-amphibole breakdown is unlikely, as was noted by Inoue *et al.* (1998).

Stability of hydrous potassic phases along the ACMA

Experiments of this study combined with those by Konzett *et al.* (1997) indicate that in peralkaline bulk compositions hydrous potassic phases break down at temperatures slightly below an ACMA defined by 17·9 GPa and 1475°C for the β → γ transition in Mg_2SiO_4 and 23·2 GPa and 1530°C for the γ → perovskite + magnesiowüstite transition (see Agee, 1998). Because the breakdown of HPPs in the peralkaline KNCMASH system occurs ~50–100°C below the ACMA, only large amounts of F can stabilize HPPs along the ACMA (Foley, 1991). Otherwise, a hydrous melt will carry most of the K under P–T conditions of an ACMA, and the K content of the solid residue will reflect partitioning between high-Ca clinopyroxene and melt. In run Ma104M at 13 GPa

Table 6: Average analyses of garnet

Exp.:	JKW19	JKW13	JKW15	JKW18	JKW17	Ma88sB	JKW29	JKW33	JKW30	JKW41	JKW47	JKW64	JKW61	JKW54
Bulk:	per	per	per	per	per	per	sub	sub	sub	sub	sub	sub	sub	sub
P (GPa):	10	10	10	10	11	13	14	14	13	13	20	20	23	23
T (°C):	1100	1200	1300	1350	1300	1100	1100	1400	1100	1300	1500	1600	1500	1700
No. of analyses:	6	7	7	5	8	9	7	6	5	5	5	10	11	10
SiO_2	42·5(3)	42·3(4)	42·1(3)	43·7(2)	43·4(4)	46·6(4)	47·8(3)	46·6(5)	46·9(3)	46·1(2)	51·6(1)	53·2(9)	49·6(3)	51·6(4)
Al_2O_3	23·1(3)	23·3(2)	22·9(2)	23·2(1)	23·2(2)	22·2(9)	19·7(5)	19·8(5)	21·6(2)	20·0(1)	13·4(5)	11·1(9)	18·7(3)	15·5(7)
MgO	19·3(8)	18·1(6)	15·8(3)	23·0(5)	21·1(7)	25·4(5)	26·2(5)	26·9(6)	25·6(4)	26·4(3)	26·4(4)	29·6(8)	28·3(2)	29·5(3)
CaO	13·7(9)	14·9(9)	18·2(4)	9·3(6)	11·4(9)	7·2(9)	6·6(4)	5·7(4)	6·9(3)	6·0(1)	6·1(2)	6·4(4)	3·4(2)	3·7(2)
Na_2O	0·1(1)	0·1(0)	<0·05	0·1(0)	0·1(1)	0·4(1)	0·5(1)	0·3(0)	0·3(0)	0·3(0)	1·7(1)	0·9(0)	1·0(1)	1·0(0)
K_2O	<0·05	<0·05	<0·05	<0·05	<0·05	<0·05	<0·05	<0·05	<0·05	<0·05	<0·05			
Σ	98·7(6)	98·7(6)	99·0(6)	99·4(2)	99·1(5)	101·8(5)	100·9(4)	99·3(5)	101·2(4)	98·9(4)	99·2(1)	101·2(5)	101·0(4)	101·3(3)
Si	3·01(2)	3·01(1)	3·01(1)	3·03(1)	3·06(1)	3·13(3)	3·24(1)	3·20(2)	3·17(1)	3·19(1)	3·55(3)	3·59(6)	3·32(1)	3·45(3)
Al	1·93(2)	1·95(2)	1·93(1)	1·90(1)	1·91(1)	1·76(7)	1·58(4)	1·60(5)	1·72(2)	1·63(1)	1·09(5)	0·89(1)	1·48(2)	1·22(5)
Mg	2·04(7)	1·92(6)	1·69(4)	2·39(5)	2·21(7)	2·55(5)	2·64(5)	2·75(5)	2·57(3)	2·71(2)	2·71(1)	2·98(8)	2·83(2)	2·94(3)
Ca	1·04(8)	1·14(7)	1·40(3)	0·69(5)	0·85(7)	0·52(7)	0·48(3)	0·42(3)	0·50(2)	0·45(1)	0·45(1)	0·46(3)	0·24(1)	0·27(1)
Na	0·01(1)	0·01(0)	—	0·01(0)	0·01(1)	0·05(1)	0·07(1)	0·05(0)	0·04(0)	0·04(0)	0·22(1)	0·11(1)	0·13(1)	0·13(1)
Σ	8·03(2)	8·02(0)	8·03(1)	8·03(1)	8·01(1)	8·01(1)	8·01(2)	8·02(1)	7·99(1)	8·02(1)	8·02(1)	8·02(1)	8·00(1)	8·00(1)
Ca/(Ca+Mg)	0·34(2)	0·37(2)	0·45(1)	0·22(1)	0·28(2)	0·17(1)	0·15(1)	0·13(1)	0·16(1)	0·14(0)	0·14(0)	0·14(1)	0·11(1)	0·11(1)
ppm K	—	—	—	—	—	—	—	—	—	—	—	296(102)	449(157)	728(375)

Garnet formulae recalculated to 12 oxygens. Lower limit of detection for K: JKW54 240 ppm; JKW61 230 ppm; JKW64: 190 ppm.

Table 7: Average analyses of high-Ca clinopyroxene

Exp.:	JKW19	JKW13	JKW15	JKW18	JKW17	JKW9	Ma88sB	Ma91B	Ma92B	Ma102M	Ma104M
Bulk:	per	per	per	per	per	per	per	per	per	per	per
P (GPa):	10	10	10	10	11	12	13	14	15	18	13
T (°C):	1100	1200	1300	1350	1300	1300	1100	1100	1100	1300	1400
No. of analyses:	8	12	7	8	8	7	10	12	11	4	4
SiO_2	55·4(4)	55·4(4)	55·2(3)	55·2(5)	55·0(2)	55·7(1)	56·4(2)	55·8(5)	56·8(2)	56·1(7)	57·5(5)
Al_2O_3	3·9(5)	3·2(6)	2·8(5)	4·4(7)	3·3(3)	3·8(8)	3·5(5)	3·8(4)	3·9(5)	1·2(4)	2·8(1)
MgO	16·2(5)	16·7(5)	16·8(5)	16·4(7)	17·1(2)	16·9(4)	17·7(6)	17·0(4)	17·6(3)	19·2(6)	22·3(3)
CaO	21·0(5)	21·7(8)	22·3(5)	19·7(6)	21·2(2)	19·7(7)	20·3(3)	20·2(4)	19·5(7)	22·0(6)	16·4(3)
Na_2O	2·5(3)	1·8(4)	1·6(3)	2·6(5)	1·9(1)	2·2(2)	2·2(2)	2·5(2)	2·6(4)	0·9(2)	1·6(1)
K_2O	0·2(1)	0·3(1)	0·3(0)	0·5(1)	0·5(0)	0·8(1)	0·5(1)	0·5(1)	0·4(1)	0·6(1)	0·5(0)
Σ	99·2(6)	99·0(4)	99·0(4)	98·8(6)	98·9(3)	99·1(4)	100·6(5)	99·8(7)	100·8(3)	100·0(8)	101·0(6)
Si	1·99(1)	2·00(1)	2·00(1)	1·99(0)	1·99(0)	2·00(1)	2·00(0)	1·99(0)	2·00(0)	2·01(1)	2·00(1)
Al	0·17(2)	0·13(3)	0·12(2)	0·18(3)	0·14(1)	0·16(2)	0·15(2)	0·16(2)	0·16(2)	0·05(2)	0·11(0)
Mg	0·87(3)	0·90(3)	0·91(3)	0·88(4)	0·92(1)	0·91(2)	0·93(3)	0·90(3)	0·93(2)	1·02(3)	1·16(2)
Ca	0·81(2)	0·84(3)	0·86(2)	0·76(3)	0·82(1)	0·76(2)	0·77(1)	0·77(2)	0·74(3)	0·84(2)	0·61(1)
Na	0·17(2)	0·12(3)	0·11(2)	0·18(3)	0·13(1)	0·16(2)	0·15(2)	0·17(2)	0·18(2)	0·06(1)	0·11(0)
K	0·01(0)	0·02(0)	0·01(0)	0·02(1)	0·02(0)	0·04(1)	0·02(0)	0·02(3)	0·02(2)	0·03(0)	0·02(0)
Σ	4·02(1)	4·01(1)	4·01(0)	4·02(0)	4·01(0)	4·01(1)	4·02(1)	4·02(5)	4·02(2)	4·01(1)	4·01(1)
K/(K+Na)	0·06(1)	0·11(2)	0·09(0)	0·11(2)	0·14(1)	0·19(4)	0·14(1)	0·10(1)	0·09(2)	0·31(2)	0·16(1)

Table 7: continued

Exp.:	JKW7	JKW14	JKW25	Ma95sB	Ma94sB	JKW29	JKW41	JKW33	JKW34	JKW30
Bulk:	per	per	per	sub	sub	sub	sub	sub	sub	sub
P (GPa):	14	14	15	10	15	14	13	14	14	13
T (°C):	1300	1200	900	1100	1100	1100	1300	1400	900	1100
No. of analyses:	6	11	5	6	5	9	6	7	6	5
SiO_2	55·8(4)	55·4(6)	56·0(5)	55·8(2)	56·8(3)	56·8(3)	56·1(2)	56·0(3)	55·7	55·6(2)
Al_2O_3	3·2(3)	2·5(5)	0·4(3)	2·8(4)	3·7(5)	3·3(3)	3·3(2)	2·9(2)	4·9	2·4(3)
MgO	18·2(4)	17·6(6)	19·3(7)	18·4(5)	18·2(7)	17·3(5)	17·8(2)	18·6(2)	15·4	17·6(2)
CaO	20·0(2)	21·4(6)	24·3(6)	21·1(4)	19·0(8)	20·5(4)	19·0(2)	19·6(5)	18·4	21·3(5)
Na_2O	2·1(2)	1·7(4)	0·3(3)	1·6(2)	2·5(4)	2·2(2)	2·0(2)	1·8(2)	3·2	1·6(2)
K_2O	0·4(0)	0·4(1)	0·2(0)	0·3(0)	0·4(1)	0·3(1)	0·7(3)	0·6(0)	0·6	0·4(1)
Σ	99·9(3)	99·0(7)	100·5(8)	100·0(3)	100·6(4)	100·3(4)	98·9(3)	99·6(6)	98·2	98·9(3)
Si	1·99(1)	2·00(1)	2·00(1)	1·99(1)	2·00(1)	2·01(0)	2·01(0)	2·00(0)	2·01	2·01(0)
Al	0·14(1)	0·11(2)	0·02(2)	0·12(2)	0·15(2)	0·14(1)	0·14(1)	0·12(1)	0·21	0·10(1)
Mg	0·97(2)	0·95(3)	1·03(4)	0·98(3)	0·96(4)	0·91(3)	0·95(1)	0·99(1)	0·83	0·95(1)
Ca	0·77(1)	0·83(2)	0·93(3)	0·80(2)	0·72(3)	0·78(2)	0·73(1)	0·75(2)	0·71	0·82(2)
Na	0·14(2)	0·12(3)	0·02(2)	0·11(1)	0·17(3)	0·15(2)	0·14(1)	0·13(1)	0·22	0·11(1)
K	0·02(0)	0·02(0)	0·01(0)	0·01(1)	0·02(1)	0·01(0)	0·03(0)	0·03(0)	0·03	0·02(0)
Σ	4·02(1)	4·01(1)	4·01(1)	4·02(1)	4·02(0)	4·00(1)	4·00(1)	4·02(1)	4·01	4·01(0)
K/(K + Na)	0·10(1)	0·15(4)	0·34(2)	0·11(1)	0·10(2)	0·08(1)	0·18(1)	0·19(1)	0·12	0·15(1)

Clinopyroxene formulae recalculated to 6 oxygens.

Table 8: Average and representative analyses of Ca-perovskite and K-hollandite

Exp.:	JKW16		JKW64	JKW54		JKW61	
Bulk:	per		sub	sub		sub	
P (GPa):	20·0		20·0	23·0		23·0	
T (°C):	1300		1600	1700		1500	
Phase:	Ca-perov	K-holl	Ca-perov	K-holl	Ca-perov	K-holl	Ca-perov
No. of analyses:		3			4	4	6
SiO_2	50·6	66·5(7)	42·3	64·9	46·0(8)	64·5(3)	45·6(9)
Al_2O_3	0·3	17·4(4)	4·6	17·2	2·1(2)	18·0(3)	1·8(2)
MgO	0·3	0·8(4)	0·5	0·7	0·3(1)	0·5(5)	0·2(1)
CaO	46·5	0·2(1)	35·5	0·1	42·9(9)	0·1(1)	44·6(1)
Na_2O	<0·05	0·1(1)	0·5	0·1	0·4(1)	0·1(0)	0·3(1)
K_2O	1·0	16·7(1)	0·4	16·6	0·4(2)	16·7(1)	0·5(3)
Σ	99·0	101·6(5)	83·8	99·5	92·0(1)	99·9(3)	92·8(1)
Si	0·99	3·02(1)	0·96	3·02	0·97(1)	2·99(1)	0·96(0)
Al	0·01	0·93(2)	0·12	0·94	0·05(1)	0·98(1)	0·05(1)
Mg	0·01	0·05(3)	0·02	0·05	0·01(0)	0·03(4)	0·01(0)
Ca	0·98	0·01(1)	0·86	0·01	0·97(1)	0·01(1)	1·00(1)
Na	—	0·01(1)	0·02	0·01	0·02(1)	0·01(0)	0·01(1)
K	0·03	0·97(1)	0·01	0·99	0·01(1)	0·99(1)	0·01(1)
Σ	2·02	5·00(2)	2·00	5·01	2·02(6)	5·02(2)	2·03(1)

K-hollandite and Ca-perovskite formulae recalculated to 2 and 8 oxygens, respectively.

and 1400°C the quench has 6·6 ± 0·5 wt % K_2O (n = 3) compared with 0·45 ± 0·02 wt % K_2O in high-Ca clinopyroxene with a resulting $D_K^{hiCapx-liquid}$ of 0·07 (because of the possibility that H_2O-soluble K-rich material was lost from the quench as a result of H_2O saturation, the D value has to be considered a maximum value). This value is consistent with $D_K^{hiCapx-liquid}$ of 0·02–0·15 obtained by Luth (1997) and Tsuruta & Takahashi (1998) from experiments in a simplified phlogopite + diopside and a dry natural alkali basalt system. In our experiments the K content of high-Ca clinopyroxene is <0·7 wt % K_2O, even at P = 18 GPa. This is consistent with the hypothesis of Luth (1997) that in a peridotitic bulk composition high-Ca clinopyroxene cannot accommodate significant K in the presence of an HPP (either solid or melt). The formation of K-rich (up to 1·7 wt % K_2O; Harlow & Veblen, 1991) high-Ca clinopyroxene found as diamond inclusions probably requires the presence of C- and K-rich (carbonatitic) melts as suggested by Harlow (1997). In metabasaltic compositions, however, omphacitic high-Ca clinopyroxene coexisting with phengite can accommodate up to 1·1 wt % K_2O (Schmidt, 1996).

In the subalkaline bulk composition, the stability of HPPs extends to temperatures significantly higher than those of an ACMA, above the solidus of H_2O-bearing peridotite (Fig. 3; Kawamoto *et al.*, 1996; Kawamoto & Holloway, 1997). Luth (1997) reported the assemblage phase X + olivine + garnet + clinopyroxene + liquid at 11 GPa and 1600°C, which suggests a potential supersolidus stability of phase X. In our experiments, phase X coexists with small amounts of quench over a temperature interval of at least 200°C. The textures do not demonstrate whether the quench formed by crystallization from a hydrous melt or a solute-rich fluid, and changes in X_{Mg} of the phases as a result of the presence of melt (Kawamoto *et al.*, 1996) could not be used in the KNCMASH system. Nevertheless, our data indicate that phase X is stable under the P–T conditions of convecting mantle, and that it coexists with hydrous peridotite melt over a wide pressure range. Thus, a supersolidus stability of phase X should control the large ion lithophile element (LILE) budget of coexisting partial melts. Although no trace element partition coefficients exist for phase X, it should, like other HPPs, store and retain large ions such as Cs, Rb, Ba or Pb in the

Table 9: Representative analyses of coexisting phases from natural KLB-1 + 10% Kr

Exp.:	JKW64					JKW69				
P (GPa):	12·0					14·0				
T (°C):	1200					1200				
	ga	ol	hiCapx	loCapx	Kr	ga	β*	hiCapx	loCapx	pX
SiO_2	42·5	40·8	52·4	58·4	56·6	44·2	40·7	51·8	55·4	45·4
TiO_2	0·1	<0·05	0·3	<0·05	0·1	0·3	<0·05	0·6	0·1	0·2
Cr_2O_3	2·4	<0·05	0·7	<0·05	0·1	1·6	0·1	0·8	0·3	0·5
Al_2O_3	21·2	<0·05	6·8	0·1	0·8	18·6	0·1	7·1	3·7	0·5
Fe_2O_3	1·9	—	2·0	1·1	1·9	4·4	—	2·5	2·4	—
FeO	7·8	9·3	1·5	4·3	0·6	3·1	10·9	1·0	2·2	6·7
MnO	<0·05	0·1	0·1	0·1	0·1	0·5	0·1	<0·05	0·2	0·1
MgO	20·8	50·3	15·2	36·3	22·7	23·1	49·1	15·2	34·1	28·3
NiO	<0·05	0·4	<0·05	0·2	0·1	<0·05	0·4	<0·05	0·1	<0·05
CaO	3·9	<0·05	19·8	0·2	5·8	4·9	<0·05	20·0	1·4	0·3
Na_2O	0·2	<0·05	1·9	0·05	3·9	0·5	0·1	1·9	0·3	1·5
K_2O	<0·05	<0·05	<0·05	<0·05	6·0	<0·05	<0·05	0·1	<0·05	14·5
H_2O	—	—	—	—	2·2	—	—	—	—	
Σ	101·0	100·8	100·6	100·7	100·9	101·2	101·4	100·9	100·2	97·9
Si	3·01	0·99	1·88	1·99	7·89	3·09	0·99	1·86	1·90	
Ti	0·01	—	0·01	—	0·01	0·02	—	0·02	0·00	
Cr	0·13	—	0·02	—	0·01	0·09	0·00	0·02	0·01	
Al	1·77	—	0·29	0·00	0·13	1·54	0·00	0·30	0·15	
Fe^{3+}	0·10	—	0·06	0·03	0·20	0·23	—	0·07	0·06	
Fe^{2+}	0·46	0·19	0·04	0·12	0·07	0·18	0·22	0·03	0·06	
Mn	0·02	0·00	0·00	0·00	0·01	0·03	0·00	—	0·01	
Mg	2·19	1·82	0·81	1·84	4·71	2·40	1·77	0·81	1·74	
Ni	—	0·01	—	0·01	0·02	—	0·01	—	0·00	
Ca	0·30	—	0·76	0·01	0·87	0·37	—	0·77	0·05	
Na	0·02	—	0·13	0·00	1·04	0·06	0·00	0·13	0·02	
K	—	—	—	—	1·07	—	—	0·00	—	
$X_{Mg}(Fe_{tot})$	0·80	0·90	0·90	0·93	0·95	0·85	0·89	0·89	0·93	0·88
K/(K + Na)	—	—	0·02	—	0·51	—	—	0·03	—	0·87

Mineral formulae recalculated as follows: α/β-Mg_2SiO_4 3 cat/4 ox; pyroxenes 4 cat/6 ox; ga 8 cat/12 ox; Kr 16 cat/23 ox + 2 OH.
*Verified by Raman spectroscopy.

large potassium lattice position (Kramers *et al.*, 1983; Rosenbaum, 1993; Irifune *et al.*, 1994; Ionov *et al.*, 1997).

Potassium recycling in subduction zones

Experimental studies suggest that within subducted oceanic crust [mid-ocean ridge basalt (MORB), andesites, graywackes] the major subsolidus potassium carrier is phengite, which is stable to 10 GPa and breaks down to form K-hollandite + K-rich fluid at P >10 GPa (Domanik & Holloway, 1996; Schmidt, 1996). K-feldspar would survive initial stages of subduction only under fluid-absent conditions but could react to form K-cymrite (hydrous hexasanidine $KAlSi_3O_8.nH_2O$) under fluid-present conditions and remain stable in the hydrated form to 8 GPa (George E. Harlow, personal communication, 1999). Thus, potassium and water transport are likely to be coupled to 300 km depths in Al-rich metasedimentary bulk compositions. Dehydration and/or melting reactions within the slab involving HPPs such as continuous phengite dehydration, K-MORB melting or Ca-amphibole

and phlogopite breakdown at <3 GPa (Domanik & Holloway, 1996; Schmidt, 1996) can provide K and H_2O and stabilize HPPs within the peridotitic mantle wedge. With increasing *P*, the succession is phlogopite ($\pm$ Ca-amphibole) $\rightarrow$ K-richterite $\rightarrow$ phase X, with final dehydration of phase X to K-hollandite at $P \geq 20$ GPa or 600 km. Decoupling of K and H_2O in the mantle wedge therefore will occur at the base of the transition zone, or 300 km deeper than in the subducting slab. Any K transferred to the mantle wedge below 150 km will be lost for recycling by arc magmatism, and dragged down into the lower mantle in K-hollandite.

For most subduction zone geometries (see Davies & Stevenson, 1992; Schmidt & Poli, 1998) the partially molten zone that feeds arc volcanism lies above a region of the mantle wedge in which phlogopite is stable. Xenolithic evidence (e.g. Swanson *et al.*, 1987; Canil & Scarfe, 1988; McGibbon *et al.*, 1988; Ionov & Hofmann, 1995; Ertan & Leeman, 1996) confirms the presence of phlogopite in subarc mantle. Assuming that isotherms parallel the subducting slab, it is difficult to transport phlogopite-bearing peridotite into the melting zone of the wedge (>1200°C at 3 GPa for phlogopite melting; see Wendlandt & Eggler, 1980). Lateral transport of phlogopite through a mechanism such as that proposed by Davies & Stevenson (1992) for amphibole is unsuitable because of the much higher *P* stability of phlogopite compared with amphibole. On the basis of experimentally derived partition coefficients, LaTourrette *et al.* (1995) showed that phlogopite in the residue of an arc magma would be inconsistent with typical trace element patterns of arc lavas (e.g. Saunders *et al.*, 1991) because residual phlogopite would strongly retain LILE. Thus, the enrichment in LILE of arc lavas might be due to either complete extraction of phlogopite with the degree of LILE enrichment controlled by the modal amount of phlogopite in the source or by addition of LILE-enriched melts or fluids rising from the slab through channels without pervasive phlogopite formation.

ACKNOWLEDGEMENTS

Part of the multianvil experiments were performed at the Bayerisches Geoinstitut under the EC 'Human Capital and Mobility—Access to Large Scale Facilities' programme (Contract ERBCHGECT940053 to D. C. Rubie). Sincere thanks go to Dave Rubie for providing access to the high-pressure equipment, and especially to Max Schmidt for sacrificing his time and nerves in an effort to protect the equipment from destruction while it was being used by J.K. We would also like to thank Bjørn Mysen for his help with Raman spectroscopy, and Hexiong Yang for helpful comments on an early version of the manuscript. Eiichi Takahashi kindly provided a sample of KLB-1. Reviews by George Harlow, Bob Luth, and Anne Peslier helped to improve the manuscript and are gratefully acknowledged. This work was supported by the Swiss National Science Foundation, the NSF Center for High Pressure Research, and the Carnegie Institution of Washington.

REFERENCES

Agee, C. B. (1998). Phase transformations and seismic structure in the upper mantle and transition zone. In: Hemley, R. J. (ed.) *Ultrahigh-Pressure Mineralogy: Physics and Chemistry of the Earth's Deep Interior. Mineralogical Society of America, Reviews in Mineralogy* **37**, 165–203.

Andrault, D., Neuville, D. R., Flank, A.-M. & Wang, Y. (1998). Cation sites in Al-rich $MgSiO_3$ perovskites. *American Mineralogist* **83**, 1045–1053.

Basu, A. R. (1978). Trace elements and Sr-isotopes in some mantle-derived hydrous minerals and their significance. *Geochimica et Cosmochimica Acta* **42**, 659–668.

Bertka, C. M. & Fei, Y. (1997). Mineralogy of the Martian interior up to core–mantle boundary pressures. *Journal of Geophysical Research* **102**, 5251–5264.

Canil, D. & Scarfe, C. M. (1988). Origin of phlogopite in mantle xenoliths from Kostal Lake, Wells Gray Park, British Columbia. *Journal of Petrology* **30**, 1159–1179.

Davies, J. H. & Stevenson, D. J. (1992). Physical model for the source region of subduction zone volcanics. *Journal of Geophysical Research* **97**, 2037–2070.

Dawson, J. B. & Smith, J. V. (1977). The MARID (mica–amphibole–rutile–ilmenite–diopside) suite of xenoliths in kimberlite. *Geochimica et Cosmochimica Acta* **41**, 309–323.

Domanik, K. J. & Holloway, J. R. (1996). The stability and composition of phengitic muscovite and associated phases from 5·5 to 11 GPa: implications for deeply subducted sediments. *Geochimica et Cosmochimica Acta* **60**, 4133–4151.

Ertan, I. E. & Leeman, W. P. (1996). Metasomatism of Cascades subarc mantle: evidence from a rare phlogopite orthopyroxenite xenolith. *Geology* **24**, 451–454.

Esperança, S. & Holloway, J. R. (1987). On the origin of some mica-lamprophyres: experimental evidence from a mafic minette. *Contributions to Mineralogy and Petrology* **95**, 207–216.

Finger, L. W., Yang, H., Konzett, J. & Fei, Y. (1998). The crystal structure of a new clinopyribole, a high-pressure potassic phase. *EOS Transactions, American Geophysical Union* **79**(17), S161.

Foley, S. (1991). High-pressure stability of the fluor- and hydroxy-endmembers of pargasite and K-richterite. *Geochimica et Cosmochimica Acta* **55**, 2689–2694.

Foley, S. F. (1992). Vein-plus-wall-rock melting mechanisms in the lithosphere and the origin of potassic alkaline magmas. *Lithos* **28**, 435–453.

Foley, S. F., Jenner, G. A., Konzett, J. & Sweeney, R. J. (1995). Trace element partitioning in natural phlogopite- and K-richterite-bearing xenoliths from southern African kimberlites. *Sixth International Kimberlite Conference Extended Abstracts*. Novosibirsk: United Institute of Geology, Geophysics and Mineralogy, Siberian Branch of Russian Academy of Sciences, pp. 164–166.

Frost, D. J. & Fei, Y. (1998). Stability of phase D at high pressure and high temperatures. *Journal of Geophysical Research* **103**, 7463–7474.

Gasparik, T. (1989). Transformation of enstatite–diopside–jadeite pyroxenes to garnet. *Contributions to Mineralogy and Petrology* **102**, 389–405.

Gilbert, M. C. & Briggs, D. F. (1974). Comparison of the stabilities of OH- and F-potassic richterites—a preliminary report. *Transactions of the American Geophysical Union* **55**, 480–481.

Harlow, G. E. (1997). K in clinopyroxene at high pressure and temperature: an experimental study. *American Mineralogist* **82**, 259–269.

Harlow, G. E. & Veblen, D. R. (1991). Potassium in clinopyroxene: inclusions from diamonds. *Science* **251**, 652–655.

Inoue, T., Irifune, T., Yurimoto, H. & Miyagi, I. (1995*a*). Decomposition of K-amphibole at high pressure: implications for the origin of the third chain volcanism. *EOS Transactions, American Geophysical Union* **76**, F711.

Inoue, T., Yurimoto, H. & Kudoh, Y. (1995*b*). Hydrous modified spinel $Mg_{1·75}SiH_{0·5}O_4$: a new water reservoir in the mantle transition region. *Geophysical Research Letters* **22**, 117–120.

Inoue, T., Irifune, T., Yurimoto, H. & Miyagi, I. (1998). Decomposition of K-amphibole at high pressures and implications for subduction zone volcanism. *Physics of the Earth and Planetary Interiors* **107**, 221–231.

Ionov, D. A. & Hofmann, A. W. (1995). Nb–Ta-rich mantle amphiboles and micas: implications for subduction-related metasomatic trace element fractionation. *Earth and Planetary Science Letters* **131**, 341–356.

Ionov, D. A., Griffin, W. L. & O'Reilly, S. O. (1997). Volatile-bearing minerals and lithophile trace elements in the upper mantle. *Chemical Geology* **141**, 153–184.

Irifune, T., Ringwood, A. E. & Hibberson, W. O. (1994). Subduction of continental crust and terrigenous and pelagic sediments: an experimental study. *Earth and Planetary Science Letters* **126**, 351–368.

Ito, E. & Takahashi, E. (1989). Postspinel transformations in the system Mg_2SiO_4–Fe_2SiO_4 and some geophysical implications. *Journal of Geophysical Research* **94**, 637–646.

Kanzaki, M. (1987). Ultrahigh-pressure phase relations in the system $Mg_4Si_4O_{12}$–$Mg_3Al_2Si_3O_{12}$. *Physics of the Earth and Planetary Interiors* **49**, 168–175.

Katsura, T. & Ito, E. (1989). The system Mg_2SiO_4–Fe_2SiO_4 at high pressures and temperatures: precise determination of stabilities of olivine, modified spinel, and spinel. *Journal of Geophysical Research* **94**, 15663–15670.

Kawamoto, T. & Holloway, J. R. (1997). Melting temperature and partial melt chemistry of H_2O-saturated mantle peridotite to 11 Gigapascals. *Science* **276**, 240–243.

Kawamoto, T., Hervig, R. L. & Holloway, J. R. (1996). Experimental evidence for a hydrous transition zone in the early Earth's mantle. *Earth and Planetary Science Letters* **142**, 587–592.

Kesson, S. E., Fitz Gerald, J. D., Shelley, J. M. G. & Withers, R. L. (1995). Phase relations, structure and crystal chemistry of some aluminous silicate perovskites. *Earth and Planetary Science Letters* **134**, 187–201.

Kohlstedt, D. L., Keppler, H. & Rubie, D. C. (1996). Solubility of water in the α, β and γ phases of $(Mg,Fe)_2SiO_4$. *Contributions to Mineralogy and Petrology* **123**, 345–357.

Konzett, J. & Fei, Y. (1998). Hydrous potassic phases at high pressures: the stability of potassium amphibole and phase X and a new ordered hydrous pyribole. *EOS Transactions, American Geophysical Union* **79**(17), S161.

Konzett, J. & Ulmer, P. (1999). The stability of hydrous potassic phases in lherzolitic mantle—an experimental study to 9·5 GPa in simplified and natural bulk compositions. *Journal of Petrology* **40**, 629–652.

Konzett, J. & Yang, H. (1998). Structure and composition of Phase X, a hydrous alkali-rich high pressure silicate. *EOS Transactions, American Geophysical Union* **45**, F996.

Konzett, J., Sweeney, R. J., Thompson, A. B. & Ulmer, P. (1997). Potassium amphibole stability in the upper mantle: an experimental study in a peralkaline KNCMASH system to 8·5 GPa. *Journal of Petrology* **38**, 537–568.

Kramers, J. D., Roddick, J. C. M. & Dawson, J. B. (1983). Trace element and isotope studies on veined, metasomatic and 'MARID' xenoliths from Bultfontein, South Africa. *Earth and Planetary Science Letters* **65**, 90–106.

Kudoh, Y., Finger, L. W., Hazen, R. M., Prewitt, C. T., Kanzaki, M. & Veblen, D. R. (1993). Phase E: a high pressure hydrous silicate with unique crystal chemistry. *Physics and Chemistry of Minerals* **19**, 357–360.

Kudoh, Y., Inoue, T. & Arashi, H. (1996). Structure and crystal chemistry of hydrous wadsleyite, $Mg_{1·75}SiH_{0·5}O_4$: possible hydrous magnesium silicate in the mantle transition zone. *Physics and Chemistry of Minerals* **23**, 461–469.

LaTourrette, T., Hervig, R. L. & Holloway, J. R. (1995). Trace element partitioning between amphibole, phlogopite, and basanite melt. *Earth and Planetary Science Letters* **135**, 13–30.

Leake, B. E. (1978). Nomenclature of amphiboles. *American Mineralogist* **63**, 1023–1053.

Leake, B. E., Woolley, A. R., Arps, C. E. S., Birch, W. D., Gilbert, M. C., Grice, J. D., Hawthorne, F. C., Kato, A., Kisch, H. J., Krivovichev, V. G., Linthout, K., Laird, J., Mandarino, J. A., Maresch, W. V., Nickel, E. H., Rock, N. M. S., Schumacher, J. C., Smith, D. C., Stephenson, N. C. N., Ungaretti, L., Whittaker, E. J. W. & Youzhi, G. (1997). Nomenclature of amphiboles: Report of the Subcommittee on Amphiboles of the International Mineralogical Association, Commission on New Minerals and Mineral Names. *American Mineralogist* **82**, 1019–1038.

Lesher, C. E. & Walker, D. (1988). Cumulate maturation and melt migration in a temperature gradient. *Journal of Geophysical Research* **93**, 10295–10311.

Libau, F. (1982). Classification of silicates. In: Ribbe, P. H. (ed.) *Ortho-Silicates. Mineralogical Society of America, Reviews in Mineralogy* **5**, 1–24.

Luth, R. W. (1995). Potassium in pyroxenes at high pressure. *EOS Transactions, American Geophysical Union* **76**, F711.

Luth, R. W. (1997). Experimental study of the system phlogopite–diopside from 3·5 to 17 GPa. *American Mineralogist* **82**, 1198–1209.

Massonne, H.-J. (1992). Evidence for low-temperature ultrapotassic siliceous fluids in subduction zone environments in the system K_2O–MgO–Al_2O_3–SiO_2–H_2O (KMASH). *Lithos* **28**, 421–435.

Massonne, H.-J. & Schreyer, W. (1989). Stability field of the high-pressure assemblage talc + phengite and two new phengite barometers. *European Journal of Mineralogy* **1**, 391–410.

McGibbon, F. M., Hawkesworth, C. J. & Menzies, M. A. (1988). Metasomatic or intercumulus origin of phlogopite in glimmerites from Foster Crater, Antarctica. *Chemical Geology* **70**, 12.

Mengel, K. & Green, D. H. (1989). Stability of amphibole and phlogopite in metasomatised peridotite under water-saturated and water-undersaturated conditions. In: Ross, J. (ed.) *Fourth International Kimberlite Conference. Australian Journal of Earth Sciences Special Publication* **14**, 571–581.

Mitchell, R. H. (1995). *Kimberlites, Orangeites and Related Rocks*. New York: Plenum, 410 pp.

Mitchell, R. H. & Bergman, S. C. (1991). *Petrology of Lamproites*. New York: Plenum, 447 pp.

Morishima, H., Kato, T., Suto, M., Ohtani, E., Urakawa, S., Utsumi, W., Shimomura, O. & Kikegawa, T. (1994). The phase boundary between α- and β-Mg_2SiO_4 determined by *in situ* X-ray observation. *Science* **265**, 1202–1203.

Oguri, K., Funamori, N., Sakai, F., Kondo, T., Uchida, T. & Yagi, T. (1997). High-pressure and high-temperature phase relations in diopside $CaMgSi_2O_6$. *Physics of the Earth and Planetary Interiors* **104**, 363–370.

Ringwood, A. E. (1967). Pyroxene–garnet transformations in the Earth's mantle. *Earth and Planetary Science Letters* **2**, 255–263.

Ringwood, A. E. & Major, A. (1971). Synthesis of majorite and other high pressure garnets and perovskites. *Earth and Planetary Science Letters* **12**, 411–418.

Rogers, N. W. (1992). Potassic magmatism as a key to trace-element enrichment processes in the upper mantle. *Journal of Volcanology and Geothermal Research* **50**, 85–99.

Rosenbaum, J. M. (1993). Mantle phlogopite: a significant lead repository. *Chemical Geology* **106**, 475–483.

Rubie, D. C., Karato, S., Yan, H. & O'Neill, H. St C. (1993). Low differential stress and controlled chemical environment in multi-anvil high pressure devices. *Physics and Chemistry of Minerals* **20**, 315–322.

Sato, K. (1997). Melting experiments on a synthetic olivine lamproite composition up to 8 GPa: implications to its petrogenesis. *Journal of Geophysical Research* **102**, 14751–14764.

Sato, K., Katsura, T. & Ito, E. (1997). Phase relations of natural phlogopite with and without enstatite up to 8 GPa: implications for mantle metasomatism. *Earth and Planetary Science Letters* **146**, 511–526.

Saunders, A. D., Norry, M. J. & Tarney, J. (1991). Fluid influence on the trace element compositions of subduction zone magmas. *Philosophical Transactions of the Royal Society of London* **335**, 377–392.

Schmidt, M. W. (1993). Phase relations and compositions in tonalite as a function of pressure: an experimental study at 650°C. *American Journal of Science* **293**, 1011–1060.

Schmidt, M. W. (1996). Experimental constraints on recycling of potassium from subducted oceanic crust. *Science* **272**, 1927–1930.

Schmidt, M. W. & Poli, S. (1998). Experimentally based water budgets for dehydrating slabs and consequences for arc magma generation. *Earth and Planetary Science Letters* **163**, 361–379.

Seifert, F. & Schreyer, W. (1971). Synthesis and stability of micas in the system K_2O–MgO–SiO_2–H_2O and their relations to phlogopite. *Contributions to Mineralogy and Petrology* **30**, 196–215.

Sudo, A. & Tatsumi, Y. (1990). Phlogopite and K-amphibole in the upper mantle: implications for magma genesis in subduction zones. *Geophysical Research Letters* **17**, 29–32.

Swanson, S. E., Kay, S. M., Brearley, M. & Scarfe, C. M. (1987). Arc and back-arc xenoliths in Kurile–Kamchatka and Western Alaska. In: Nixon, P. H. (ed.) *Mantle Xenoliths*. Chichester: John Wiley, pp. 303–318.

Takahashi, E. (1986). Melting of a dry peridotite KLB-1 up to 14 GPa: implications on the origin of peridotitic upper mantle. *Journal of Geophysical Research* **91**, 9367–9382.

Taylor, W. R., Tompkins, L. A. & Haggerty, S. F. (1994). Comparative geochemistry of West African kimberlites: evidence for a micaceous kimberlite endmember of sublithospheric origin. *Geochimica et Cosmochimica Acta* **58**, 4017–4037.

Thompson, J. B. (1981). An introduction to the mineralogy and petrology of the biopyriboles. In: Veblen, D. R. (ed.) *Amphiboles and Other Hydrous Pyriboles—Mineralogy. Mineralogical Society of America, Reviews in Mineralogy* **9A**, 141–188.

Trønnes, R. G. (1990). Low-Al, high-K amphiboles in subducted lithosphere from 200–400 km depth: experimental evidence. *EOS Transactions, American Geophysical Union* **71**, 1587.

Trønnes, R. G., Takahashi, E. & Scarfe, C. M. (1988). Stability of K-richterite and phlogopite to 14 GPa. *EOS Transactions, American Geophysical Union* **69**, 1510–1511.

Tsuruta, K. & Takahashi, E. (1998). Melting study of an alkali basalt JB-1 up to 12·5 GPa: behaviour of potassium in the deep mantle. *Physics of the Earth and Planetary Interiors* **107**, 119–130.

Veblen, D. R. (1981). Non-classical pyriboles and polysomatic reactions in biopyriboles. In: Veblen, D. R. (ed.) *Amphiboles and Other Hydrous Pyriboles—Mineralogy. Mineralogical Society of America, Reviews in Mineralogy* **9A**, 189–236.

Wendlandt, R. F. & Eggler, D. H. (1980). The origins of potassic magmas: 2. Stability of phlogopite in natural spinel lherzolite and in the system $KAlSiO_4$–MgO–SiO_2–H_2O–CO_2 at high pressures and high temperatures. *American Journal of Science* **280**, 421–458.

Wilkinson, J. F. G. & Le Maitre, R. W. (1986). Upper mantle amphiboles and micas and TiO_2, K_2O, and P_2O_5 abundances and 100 Mg/(Mg + Fe^{2+}) ratios of common basalts and andesites: implications for modal mantle metasomatism and undepleted mantle compositions. *Journal of Petrology* **28**, 37–73.

Yang, H., Konzett, J., Prewitt, C. T. & Fei, Y. (1999). Single-crystal refinement of synthetic ^{M4}K-substituted potassic richterite, $K(KCa)Mg_5Si_8O_{22}(OH)_2$. *American Mineralogist* **84**, 681–685.

Young, T. E., Green, H. W., Hofmeister, A. M. & Walker, D. (1993). Infrared spectroscopic investigation of hydroxyl in β-$(Mg,Fe)_2SiO_4$ and coexisting olivine: implications for mantle evolution and dynamics. *Physics and Chemistry of Minerals* **19**, 409–422.

APPENDIX

Table A1: List of mineral end-members, abbreviations and #formulae used in this study

Mineral	Abbreviation	Formula
K-richterite	Kr	$KNaCaMg_5Si_8O_{22}(OH)_2$
phase X	pX	$KHMg_2Si_2O_7$
Na-bearing phase X	NapX	$NaHMg_2Si_2O_7$
pyrope	py	$Mg_3Al_2Si_3O_{12}$
grossular	gross	$Ca_3Al_2Si_3O_{12}$
jadeite	jad	$NaAlSi_2O_6$
diopside	di	$CaMgSi_2O_6$
clinoenstatite	cen	$Mg_2Si_2O_6$
phlogopite	phl	
pyribole	pyr	
high-Ca clinopyroxene	hiCapx	
low-Ca clinopyroxene	loCapx	
K-hollandite	K-holl	
Ca-perovskite	Ca-perov	
omphacite	omph	
garnet (majoritic)	ga	
quenched fluid or melt	Q	